

Article

Multi-UAV Optimal Mission Assignment and Path Planning for Disaster Rescue Using Adaptive Genetic Algorithm and Improved Artificial Bee Colony Method

Haoting Liu ^{1,2,*} , Jianyue Ge ¹, Yuan Wang ¹, Jiacheng Li ¹, Kai Ding ^{3,*}, Zhiqiang Zhang ², Zhenhui Guo ⁴, Wei Li ⁴ and Jinhui Lan ¹

¹ Beijing Engineering Research Center of Industrial Spectrum Imaging, University of Science and Technology, Beijing 100083, China; yueyue202011@outlook.com (J.G.); Willing20201@outlook.com (Y.W.); yyca_2015@sina.com (J.L.); jinhuilan@protonmail.com (J.L.)

² School of Electronic and Electrical Engineering, University of Leeds, Leeds LS2 9JT, UK; eenzzh@leeds.ac.uk

³ Science and Technology on Near-Surface Detection Laboratory, Wuxi 214035, China

⁴ Jiuquan Satellite Launch Center, Jiuquan 732750, China; gzh9829@sohu.com (Z.G.); liwei_20@outlook.com (W.L.)

* Correspondence: liuhaoting@ustb.edu.cn (H.L.); winfast113@sina.com (K.D.)

Abstract: An optimal mission assignment and path planning method of multiple unmanned aerial vehicles (UAVs) for disaster rescue is proposed. In this application, the UAVs include the drug delivery UAV, image collection UAV, and communication relay UAV. When implementing the modeling and simulation, first, three threat sources are built: the weather threat source, transmission tower threat source, and upland threat source. Second, a cost-revenue function is constructed. The flight distance, oil consumption, function descriptions of UAV, and threat source factors above are considered. The analytic hierarchy process (AHP) method is utilized to estimate the weights of cost-revenue function. Third, an adaptive genetic algorithm (AGA) is designed to solve the mission allocation task. A fitness function which considers the current and maximum iteration numbers is proposed to improve the AGA convergence performance. Finally, an optimal path plan between the neighboring mission points is computed by an improved artificial bee colony (IABC) method. A balanced searching strategy is developed to modify the IABC computational effect. Extensive simulation experiments have shown the effectiveness of our method.

Keywords: multiple UAVs; mission assignment; path planning; genetic algorithm; artificial bee colony; disaster rescue



Citation: Liu, H.; Ge, J.; Wang, Y.; Li, J.; Ding, K.; Zhang, Z.; Guo, Z.; Li, W.; Lan, J. Multi-UAV Optimal Mission Assignment and Path Planning for Disaster Rescue Using Adaptive Genetic Algorithm and Improved Artificial Bee Colony Method. *Actuators* **2022**, *11*, 4. <https://doi.org/10.3390/act11010004>

Academic Editor: Dario Richiedei

Received: 10 November 2021

Accepted: 15 December 2021

Published: 28 December 2021

Publisher's Note: MDPI stays neutral with regard to jurisdictional claims in published maps and institutional affiliations.



Copyright: © 2021 by the authors. Licensee MDPI, Basel, Switzerland. This article is an open access article distributed under the terms and conditions of the Creative Commons Attribution (CC BY) license (<https://creativecommons.org/licenses/by/4.0/>).

1. Introduction

Different from traditional disaster rescue applications [1] which utilize 3D terrain reconstruction or ground target recognition, the multiple unmanned aerial vehicles (UAVs)-based disaster rescue plan [2] utilizes the UAVs with distinct functions to realize people searching, complete injury identification, and provide medical assistance in the disaster zones [3]. In our past research works, a multi-UAV system is developed; this system includes [4] the drug delivery UAV, image collection UAV, and communication relay UAV. Compared with the single UAV system, the multiple UAVs can increase the resource delivery ability, intensify the flight security, and reduce the mission cost. Many factors will affect the rescue task including the environment factor [5] (such as the weather, terrain, and artificial facilities), UAV performance factor [6] (such as the maximum flight distance, oil consumption, or typical rescue function), and mission complexity itself. Currently, when implementing the disaster rescue using the multi-UAV-based system, how to assign the amount and combination mode of UAVs reasonably [7,8] and how to plan their flight paths are the issues that should be researched carefully.

Much research has been done to solve the UAV-based mission assignment and path planning tasks. In [9], a distributed control law was developed to solve the issue of mission assignment of multi-UAV. The coordination task was solved by reaching a consensus on a defined coordination state. In [10], a coordinated standoff target tracking strategy which considered the path shaping for multiple UAVs was presented. A new path shaping technique was developed in that application. In [11], online path planning for joint detection and tracking of multiple unknown radio-tagged objects was developed. This research could be used for information collection using UAVs with on-board sensors. In general, the research on mission assignment and path planning can be transferred into the optimization modelling problem [12]. To solve that problem, the proper cost-revenue function should be designed firstly, and then some optimization methods can be developed to solve it. Currently, many research studies have been done in the fields of mission assignment and path planning; however, the corresponding research in disaster rescue is still rare.

The essence of multi-UAV mission assignment and path planning is to use interactive information and data analysis measurement to realize collaborative work of UAVs. Table 1 presents an algorithm review of multi-UAV mission assignment and path planning. Regarding mission assignment, the heuristic algorithm [13–15] uses the intuitive experiences to build its computational strategy; the mathematical programming [16,17] employs the classic algebra or matrix theory to solve optimal computation with various of constraints; and the stochastic intelligent optimization [18–20] considers the typical theories, such as biological or physical rules, to accomplish optimal computation. As for path planning, the mathematical programming [21,22] can solve path generation with the consideration of environment and kinematics factors; the artificial potential field method [23,24] considers the balance between the attractive and repulsive forces to implement path searching; the graph-based method [25–28] uses the modeling and computation of graph theory to accomplish path planning; and the intelligent optimization [29,30] can carry out path creation using typical biological imitation algorithms.

In this paper, an optimal mission assignment and path planning method of multiple UAVs for the disaster rescue application is proposed. The drug delivery UAV, image collection UAV, and communication relay UAV are considered in this system. When carrying out mission assignment, first, three threat sources [31] are designed, they are the weather threat source, i.e., the wind and rain, transmission tower threat source, i.e., the electromagnetic interference disturbance, and terrain threat source, i.e., the upland. Second, a cost-revenue function is proposed. The flight distance, oil consumption, UAV function descriptions, together with the threat source factors, are all employed to construct that function. The analytic hierarchy process (AHP) method [32] is used to estimate the weights of this model. Third, an adaptive genetic algorithm (AGA) [33] is considered to estimate the optimal mission assignment. The new fitness function is proposed to improve the performance of AGA. Finally, an improved artificial bee colony (IABC)-based optimal path planning [34] for neighboring mission points is developed. The balanced searching strategy is considered for a fast optimal computation.

The main contributions of this paper include: (1) a modelling method of the multi-UAV optimal mission assignment and path planning for the disaster rescue is proposed. Three threat source factors are defined, and a new cost-revenue function is built. (2) Both an AGA and an IABC algorithms are developed. The new fitness function and the new searching strategy are proposed to improve the computational performance of AGA and IABC, respectively.

In the following sections, first, the problem formulation of multi-UAV mission assignment and path planning will be presented. Second, the optimization modelling including the threat sources, cost-revenue function, together with AGA and IABC will be introduced. Third, some experiment results, such as the evaluations of AGA and IABC or disaster rescue simulations, will be shown.

Table 1. Review of mission assignment and path planning methods.

Representative Algorithm	Algorithm Category			
	Heuristic Algorithm	Mathematical Programming	Stochastic Intelligent Optimization Method	
Mission assignment problem	Tabu search algorithm [13], simulated annealing algorithm [14], genetic algorithm (GA) [15], etc.	Enumeration algorithm [16], dynamic programming [17], etc.	Evolutionary computation [18], swarm intelligence computing [19], artificial immune algorithm [20], etc.	
Representative Algorithm	Algorithm Category			
	Mathematical Programming	Artificial Potential Field Method	Graph-Based Method	Intelligent Optimization Method
Path planning problem	Dynamic programming [21], nonlinear programming method [22], etc.	Basic artificial potential field method [23], improved artificial potential field method [24], etc.	Dijkstra algorithm [25], A* algorithm [26], Voronoi diagram method [27], probabilistic roadmaps method [28], etc.	Swarm intelligence computing [29], bionic algorithm [30], etc.

2. Problem Formulation

Figure 1 shows the sketch map of our investigated application. The multiple UAVs are used to carry out the disaster medical rescue task from a start point; and after the drug deliveries to each mission point, they will fly to a recovery point. The natural or manmade environment factors will influence the flight security of UAVs; thus, how to assign mission points to UAVs reasonably and how to plan their flight path safely, economically, and efficiently should be considered. In Figure 1, the UAVs include the drug delivery UAV, image collection UAV, and communication relay UAV. The drug delivery UAV can take the first-aid kit and necessary medical supplies to the disaster zone. The image collection UAV is equipped with various kinds of camera for video information collection. The communication relay UAV carries the communication relay device to guarantee the information transmission of entire system. Several villages locate in different sites of disaster zone; each one of them needs to be rescued by these UAVs. Many environmental factors can threaten the flight security of UAV. For example, the nimbus cloud [35] can damage the motor or sensor of UAV, and it may also contaminate the drugs. The upland may reduce the flight security of UAV. Furthermore, the transmission tower can influence the communication system of UAV. Other factors, such as the maximum flight distance or oil consumption will also affect this mission.

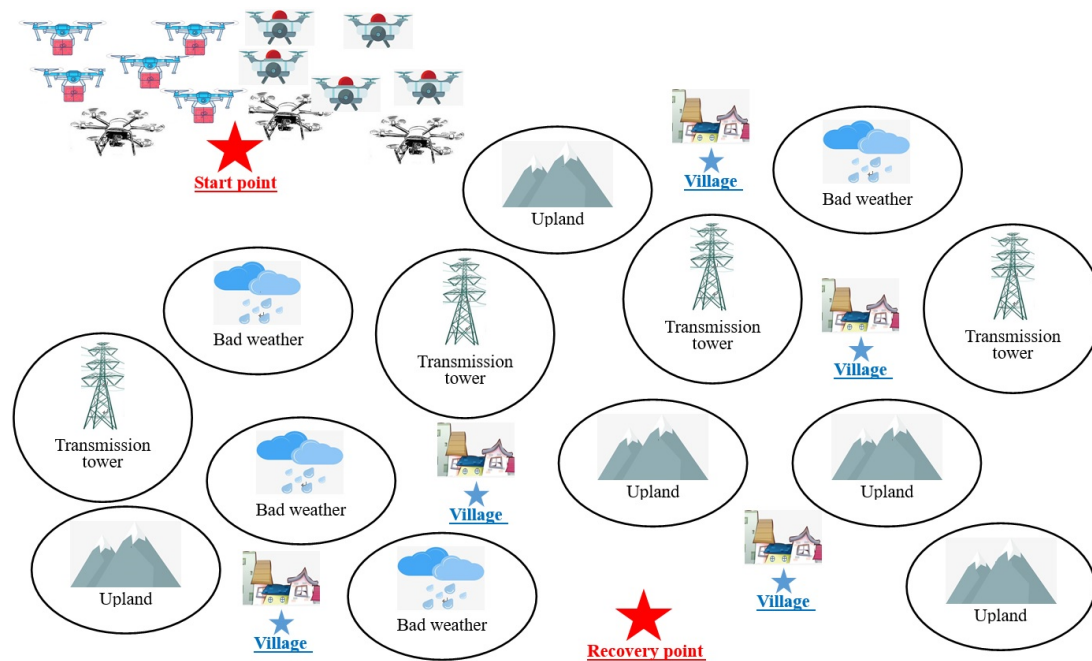


Figure 1. Sketch map of multi-UAV-based disaster rescue.

3. Optimization Modelling and Its Solution

3.1. The Proposed Computational Flow Chart

Regarding the multi-UAV-based disaster rescue, two questions should be answered. The first question is how to plan the optimal mission allocation. That means the quantity and combination mode of multiple UAVs should be designed for a rescue task. The second question is how to plan their optimal flight paths between two neighboring mission points. Many factors, such as the threat sources and flight parameters will influence the cruise path of UAV. To answer these questions, a novel method is proposed. Figure 2 shows its computational flow chart. After the threat source modelling, a cost-revenue function is designed. The AHP method is used to estimate the weights of cost-revenue function. A kind of AGA is used to solve the optimal mission assignment and an IABC is considered to estimate the optimal path between the neighboring mission points. The main inputs of this model include the amount of UAV, coordinates of mission points (the villages in

Figure 1) and threat source centers, and control parameters of AGA and IABC algorithms. The outputs of this model are the mission assignment results of UAVs and their flight paths.

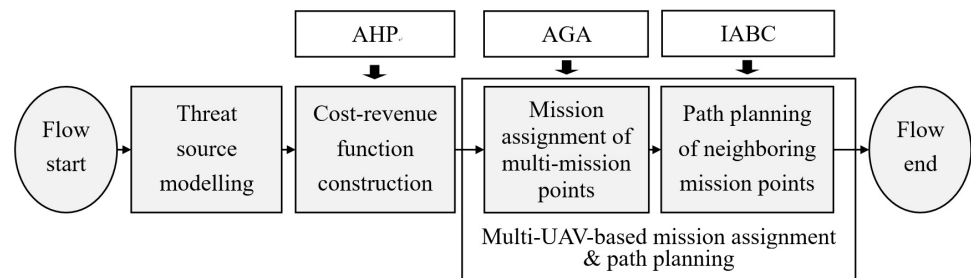


Figure 2. Proposed computational flow chart.

3.2. The Threat Source Modelling Methods

In this study, it is supposed three types of exterior threat factor will influence the UAV flight security: the severe weather, transmission tower, and upland.

(1) The severe weather threat source

In this study, the severe weather points to the wind and rain. Many methods can be used to evaluate the intensity of wind and rain in a certain area, such as the remote sensing satellite-based method [36] or atmosphere sensor-based technique [37]. Regarding the remote sensing satellite-based method, some models, such as the weather research and forecasting (WRF) model or the large Eddy simulations (LES) model [38], can be employed; however, these models are too complex for our application currently. Without loss of generality, the atmosphere observation data which are collected by the weather station are considered in this model. Figure 3 shows the 3D sketch map of weather station and the actual remote sensing map. In many cases, the weather station will be distributed in the peak of highland. Then it can assess the atmosphere state around highland. Table 2 presents the definition of wind speeds and their threat degrees. Equation (1) gives out the computational method of the severe weather threat source. In this paper, it is supposed that the 2D shape of weather threat source is a circle; the circle center is set in the weather station and the circle radius comes from the expert advice which consider the terrain and local historical climate. From Table 2 and Equation (1) it can be seen if there is a rain, the threat degree P_{WR} will be high ($P_{WR} = 1$); and if no rain appears in that zone, the threat degree would be higher with the increment of wind speed.

$$P_{i,j,p,WR} = \begin{cases} 1 & (P_{i,j,p,R} = 1) \mid (P_{i,j,p,W} = 5) \& (d_{WR} < D_{WR}) \\ 0.8 & (P_{i,j,p,R} = 0) \& (P_{i,j,p,W} = 4) \& (d_{WR} < D_{WR}) \\ 0.6 & (P_{i,j,p,R} = 0) \& (P_{i,j,p,W} = 3) \& (d_{WR} < D_{WR}) \\ 0.4 & (P_{i,j,p,R} = 0) \& (P_{i,j,p,W} = 2) \& (d_{WR} < D_{WR}) \\ 0.2 & (P_{i,j,p,R} = 0) \& (P_{i,j,p,W} = 1) \& (d_{WR} < D_{WR}) \\ 0 & otherwise \end{cases} \quad (1)$$

$$P_{i,p,WR} = \frac{1}{M_1} \sum_{j=1}^{M_1} P_{i,j,p,WR} \quad (2)$$

where $P_{i,j,p,WR}$ represents the threat degree of rain and wind, i means the i^{th} UAV, j means the j^{th} threat source, p is the p^{th} iteration number, WR indicates the wind and rain threat sources; $P_{i,j,p,R}$ and $P_{i,j,p,W}$ are the threat degrees of rain and wind, respectively; d_{WR} is the distance between the UAV and weather threat source center; D_{WR} is the radius of weather threat source; symbols “ \mid ” and “ $\&$ ” represent the relationship operators “or” and “and” between two variables; $P_{i,p,WR}$ is the integrated severe weather threat degree of the i^{th} UAV; and M_1 is the total amount of weather threat source (weather station).

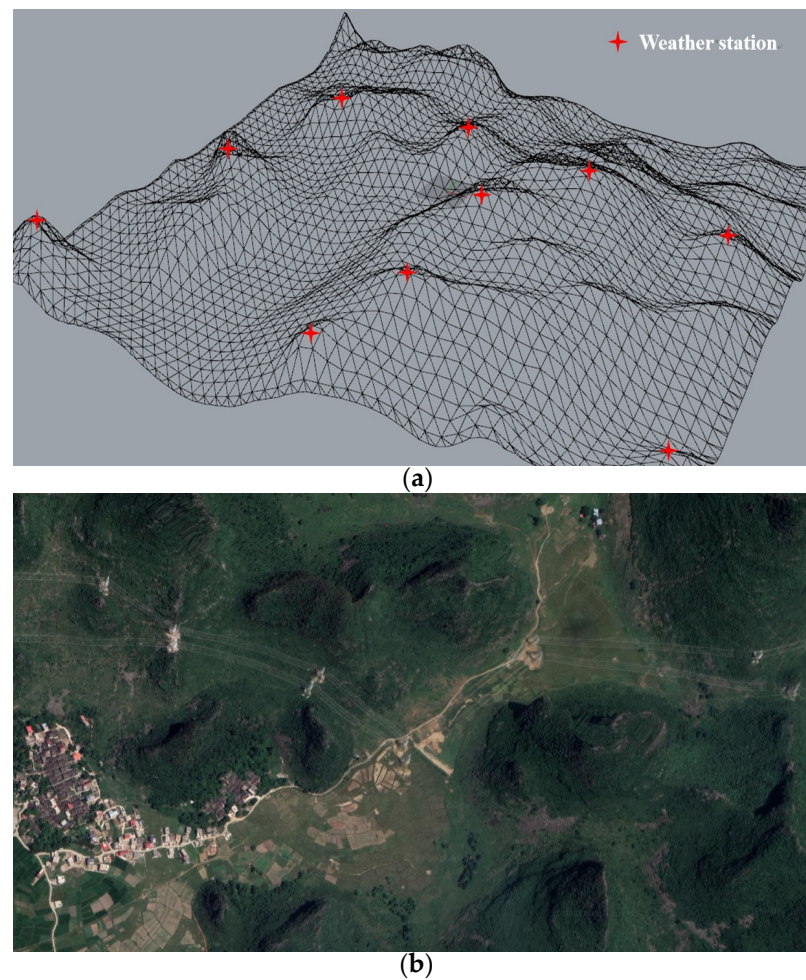


Figure 3. Sketch map of weather station and its actual remote sensing map. (a) Sketch map of weather station. (b) Actual remote sensing map which comes from Google earth (<https://www.google.com/earth/> accessed on 19 January 2020).

Table 2. Definitions of wind speeds and their threat degrees.

Wind Speed (m/s)	(0.0, 0.2]	(0.2, 7.9]	(7.9, 13.8]	(13.8, 24.4]	(24.4, 100.0]
Threat Degree	1	2	3	4	5

(2) The transmission tower threat source

The transmission tower is extensive erected in the mountain area in China which will create electromagnetic disturbance [39] to the navigation system of UAV. Although many anti-disturbance techniques have been developed to decrease that negative effect for UAV [40]; however, it is better to avoid the across-tower flight phenomenon. Figure 4 shows the sketch maps of transmission tower and a simplified model of intensity distribution of electromagnetic disturbance. In this paper, a bi-Gaussian mixed model (bi-GMM) [41] is used to construct the intensity distribution model of electromagnetic disturbance. In Figure 4a shows the sketch maps of electromagnetic radiation intensity distribution over the transmission tower from the front view and side view; Figure 4b,c is the 2D and 3D images of bi-GMM. Equations (3)–(5) are the computational methods of bi-GMM and the total electromagnetic disturbances of transmission tower.

$$f_{i,j,p,q}(x,y) = \frac{1}{2\pi\sigma_{1,i,j,p,q}\sigma_{2,i,j,p,q}\sqrt{1-\rho_{i,j,p,q}^2}} \times \exp\left\{-\frac{1}{2(1-\rho_{i,j,p,q}^2)}\left[\frac{(x-\mu_{1,i,j,p,q})^2}{\sigma_{1,i,j,p,q}^2} - \frac{2\rho_{i,j,p,q}(x-\mu_{1,i,j,p,q})(y-\mu_{2,i,j,p,q})}{\sigma_{1,i,j,p,q}\sigma_{2,i,j,p,q}} + \frac{(y-\mu_{2,i,j,p,q})^2}{\sigma_{2,i,j,p,q}^2}\right]\right\} \quad (3)$$

$$P_{i,j,p,TT} = \sum_{q=1}^2 \omega_{j,p,q} f_{i,j,p,q}(x,y) \quad (4)$$

$$P_{i,p,TT} = \frac{1}{M_2} \sum_{j=1}^{M_2} P_{i,j,p,TT} \quad (5)$$

where $f_{i,j,p,q}(x,y)$ ($q = 1, 2$) is the probability density function of bi-GMM function, i means the i^{th} UAV, j is of the j^{th} threat source (transmission tower), p is the p^{th} iteration number, q is the number of Gaussian function; $\mu_{1,i,j,p,q}$ and $\mu_{2,i,j,p,q}$ are the means, $\sigma_{1,i,j,p,q}$ and $\sigma_{2,i,j,p,q}$ are the variances, $\rho_{i,j,p,q}$ is the correlation coefficient; $P_{i,j,p,TT}$ is the security threat degree of the j^{th} transmission tower; $w_{j,p,q}$ is the weight of two Gaussian functions; TT means the transmission tower threat source; $P_{i,p,TT}$ is the integrated transmission tower threat degree of the i^{th} UAV; M_2 is the total number of transmission tower in the investigated area.

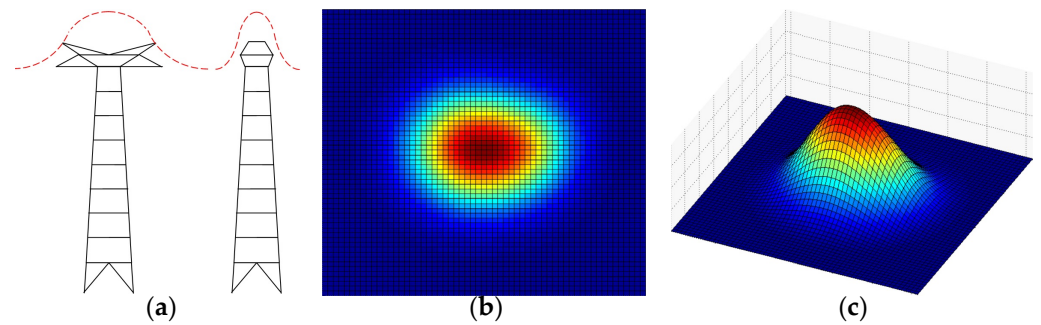


Figure 4. Sketch map of transmission tower and its simplified model of radio interference distribution. (a) Front and side views of transmission tower. (b) 2D image of bi-GMM. (c) 3D image of bi-GMM.

(3) The upland threat source

The upland will threaten the flight security of UAV because a crash may happen if the UAV is controlled improperly or flies too close to upland; therefore, the distance between the UAV and upland should affect the intensity of upland threat source. For the sake of simpleness, a circular cone model [42] is built in this study to imitate upland threat source. This kind of simplified model is like the actual terrain in China's Sichuan or Guangxi Province. Figure 5 shows the sketch map of the upland threat source model. Three situations are considered in this model. In the first situation, if the flight height of UAV is larger than the height of upland ($A_{i,j,p} > O_{i,j,p,m}$) or the maximum security flight distance of upland ($\overline{G_{i,j,p}H_{i,j,p}}$), the collision probability is 0. In the second situation, if the flight height of UAV is between the minimum security flight distance of upland ($\overline{C_{i,j,p}D_{i,j,p}}$) and the maximum security flight distance of upland ($\overline{G_{i,j,p}H_{i,j,p}}$), the collision probability will be proportional to the UAV flight height from the upland surface. In the third situation, if the flight height of UAV is lower than the minimum security flight distance of upland ($\overline{C_{i,j,p}D_{i,j,p}}$), the collision probability would be 1 in this model. From Figure 5 the larger the distance between UAV and upland surface is, the smaller the threat degree of upland would be. Equations (6)–(8) show the threat degree estimation method of one circular cone upland, some geometry relationships are employed here; and Equation (9) presents the total threat degree of multiple uplands in the disaster area.

$$C_{i,p,Total} = C_{i,p,MP} + C_{i,p,RP} \quad (10)$$

$$C_{i,p,MP} = \sum_{k=1}^K \left\{ \delta_{MP}^D P_{i,p,D}(k) + \delta_{MP}^O P_{i,p,O}(k) + (1 - t_p \times \gamma) [\delta_{MP}^{WR} P_{i,p,WR}(k) + \delta_{MP}^{TT} P_{i,p,TT}(k) + \delta_{MP}^{UT} P_{i,p,UT}(k)] \right\} \quad (11)$$

$$C_{i,p,RP} = \delta_{RP}^D P_{i,p,D}(c) + \delta_{RP}^O P_{i,p,O}(c) + (1 - t_p \times \gamma) [\delta_{RP}^{WR} P_{i,p,WR}(c) + \delta_{RP}^{TT} P_{i,p,TT}(c) + \delta_{RP}^{UT} P_{i,p,UT}(c)] \quad (12)$$

$$R_{i,p,Total} = \sum_{k=1}^K \left\{ 1 - [1 - (\alpha + s_p \times \beta)]^{r_p} \right\} \times R(k) \quad (13)$$

$$T1_{i,p} = \omega_1 C_{i,p,Total} - \omega_2 R_{i,p,Total} \quad (14)$$

$$T2_p = \sum_{i=1}^I T1_{i,p} \quad (15)$$

where $C_{i,p,Total}$ is the total cost and revenue in the p^{th} iteration computation of the i^{th} UAV; $C_{i,p,MP}$ is the cost function of the mission point; $C_{i,p,RP}$ is the cost function of the recovery point; $\delta_{MP}^D, \delta_{MP}^O, \delta_{MP}^{WR}, \delta_{MP}^{TT}, \delta_{MP}^{UT}$ are the weights of distance factor, oil consumption factor, weather threat factor, transmission tower threat factor, and upland threat factor, respectively; K is the total number of mission points; similarly, $\delta_{RP}^D, \delta_{RP}^O, \delta_{RP}^{WR}, \delta_{RP}^{TT}, \delta_{RP}^{UT}$ are the corresponding weights of recovery point; $P_{i,p,D}(k), P_{i,p,O}(k), P_{i,p,WR}(k), P_{i,p,TT}(k),$ and $P_{i,p,UT}(k)$ are the cost values of distance factor, oil consumption factor, costs of weather threat factor, transmission tower factor, and upland threat factor of the mission point k ; and $P_{i,p,D}(c), P_{i,p,O}(c), P_{i,p,WR}(c), P_{i,p,TT}(c),$ and $P_{i,p,UT}(c)$ are the corresponding cost values in recovery point; $r_p, s_p,$ and t_p are the amounts of drug delivery UAV, image collection UAV, and communication relay UAV in the p^{th} iteration, respectively; α is the parameter of drug delivery UAV which means the rate of a successful drug delivery; β is the parameter of image collection UAV which indicates the improvement probability of a drug delivery; γ is the parameter of communication relay UAV which presents the decreasing probability of all kinds of threat degrees; $R(k)$ is the revenue of the k^{th} mission point; ω_1 and ω_2 are weights, $\omega_1 = 1.0$ and $\omega_2 = 10.0$; I is the total number of UAVs.

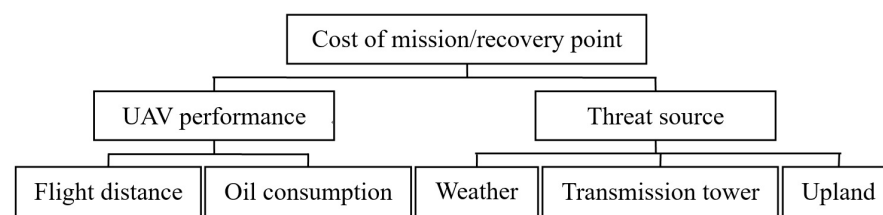


Figure 6. Hierarchy structure of AHP.

Table 3. Evaluation criterion of AHP.

Intensity of Importance	Definition
1	Equally important
3	Weakly important
5	Essentially important
7	Very strongly important
9	Absolutely important
2, 4, 6, 8	Importance between the above odd numbers

3.4. The Optimal Computational Methods: AGA and IABC

Two optimal computational methods are designed for mission assignment and path planning: an AGA is proposed for mission assignment and a kind of IABC method is considered for path planning of neighboring mission points.

- (1) The optimal mission assignment of multiple mission points using AGA
The multi-UAV can be allocated into different UAV groups by AGA to accomplish the rescue task. The computational steps of AGA are listed below.
 - (a) The population initialization. The initial population is generated, i.e., a series of initial solutions of mission assignment are created by the random number. The population size N_AGA , the current iteration number p_AGA , the maximum iteration number p_AGA_{max} , the crossing probability $P_{p_AGA,C}$, and the mutation probability $P_{p_AGA,M}$ etc., are set.
 - (b) The fitness function calculation [44]. The calculation method of the fitness function is shown by Equation (16).

$$f_{p_AGA} = T2_{p_AGA} \quad (16)$$

where f_{p_AGA} is the fitness function in the p_AGA^{th} iteration; $T2_{p_AGA}$ is defined in (15).

- (c) The iterative computation of AGA. Three kinds of computations are implemented [45]: the selection operation, crossover operation, and mutation operation. First, the selection operation considers the estimation result of fitness function, and its probability is defined in Equation (17). The roulette wheel selection method is utilized in this study. Second, the crossover processing is carried out by exchanging several gene fragments at the positions of two randomly selected individuals. Third, the mutation step is achieved by switching two genes of one randomly selected individual. The probabilities of crossover and mutation operations are defined in (18) and (19).

$$P_{p_AGA,S} = \frac{f_{p_AGA}}{\sum_{p_AGA=1}^{N_AGA} f_{p_AGA}} \quad (17)$$

$$P_{p_AGA,C} = \begin{cases} a_{p_AGA} \times \frac{P_{p_AGA,C_max}(f_{p_AGA,max} - f_{p_AGA})}{f_{p_AGA,max} - f_{p_AGA,mean}} & f_{p_AGA} \geq f_{p_AGA,mean} \\ b_{p_AGA} \times P_{p_AGA,C_max} & f_{p_AGA} < f_{p_AGA,mean} \end{cases} \quad (18)$$

$$P_{p_AGA,M} = \begin{cases} c_{p_AGA} \times \frac{P_{p_AGA,M_max}(f_{p_AGA,max} - f_{p_AGA})}{f_{p_AGA,max} - f_{p_AGA,mean}} & f_{p_AGA} \geq f_{p_AGA,mean} \\ d_{p_AGA} \times P_{p_AGA,M_max} & f_{p_AGA} < f_{p_AGA,mean} \end{cases} \quad (19)$$

where $P_{p_AGA,S}$ is the selection probability; f_{p_AGA} is the fitness function in the p_AGA^{th} iteration; N_AGA is the maximum population number; $P_{p_AGA,C}$ is the cross probability; a_{p_AGA} , b_{p_AGA} , c_{p_AGA} , and d_{p_AGA} are the control parameters in the p_AGA^{th} iteration, $a_{p_AGA} = 1.0$, $b_{p_AGA} = 1.2$, $c_{p_AGA} = 1.0$, and $d_{p_AGA} = 1.35$ in this study; P_{p_AGA,C_max} is the maximum of cross probability; $f_{p_AGA,max}$ is the maximum of fitness function; $f_{p_AGA,mean}$ is the mean of fitness function; $P_{p_AGA,M}$ is the mutation probability; P_{p_AGA,M_max} is the maximum of mutation probability.

Due to the convergence speed of traditional GA is slow with the accumulation of iteration number; an adjustment parameter is defined which is related with the iteration number. Then the new fitness function can be computed. Equations (20)–(22) present the corresponding computational methods.

$$f_{p_AGA} = K_{AGA} \times T2_{p_AGA} \quad (20)$$

$$K_{AGA} = \frac{p_AGA^{\frac{1}{h_i}}}{T2_{p_AGA}^{\max}} \quad (21)$$

$$h_i = 1 + \lg(p_AGA_{\max}) \quad (22)$$

where K_{AGA} is an adjustment parameter; h_i is a variable; $T2_{p_AGA}^{\max}$ is the maximum of cost-revenue function; p_AGA_{\max} is the maximum iteration number.

Without loss of generality, let us take the mission allocation issue of two UAV groups as an example. Figure 7 shows the sketch map of chromosome coding method [46] of proposed AGA. In Figure 7, two code sequences compose this chromosome fragment; which also means we only consider dividing the mission implementation units into two parts. Two code sequences have the equal size and the same gene definition method. For example, in the left code sequence, the first three codes indicate the amounts of drug delivery UAV, image collection UAV, and communication relay UAV, respectively; and its left codes mean the mission points which can be filled by “0” or “1”; where “0” means this UAV group will not go to this mission point, while “1” is this group will go to this mission point. Clearly, the amount of these left codes should equal to the amount of the mission point. After coding, this chromosome fragment can be used to implement the selection, crossover, and mutation operations.

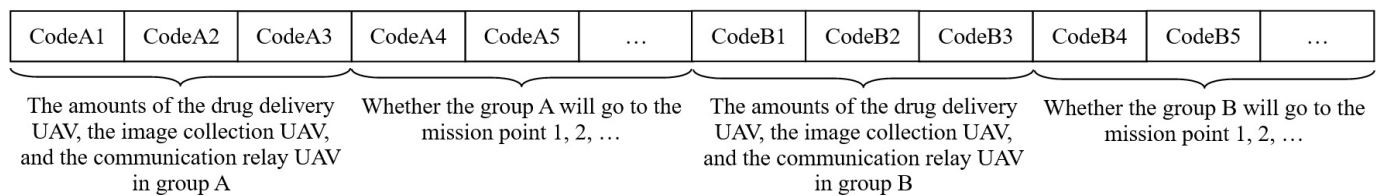


Figure 7. Sketch map of the chromosome coding method of AGA.

(2) The optimal path planning between neighboring mission points using IABC
An IABC algorithm is used to find the optimal path between neighboring mission points. The basic computational steps of artificial bee colony (ABC) algorithm are presented below.

- (a) The population initialization. The random solutions of ABC algorithm are created. The corresponding computation method [47] can be written by (23). The maximum iteration is also set, and the initial iteration number is 0.

$$x_{ij} = x_j^{\min} + \text{rand}(-1, 1) (x_j^{\max} - x_j^{\min}) \quad (23)$$

where x_{ij} is the coordinate of flight path; x_j^{\min} and x_j^{\max} are the minimum and maximum values of x_{ij} ; $i = 1, 2, \dots, NP$, and NP is the total number of bees; $j = 1, 2, \dots, D$. Here D is the dimension of estimated parameter, $D = 2$ in this study.

- (b) The path updating of employed foragers. First, the solutions v_{ij} of employed foragers can be computed by (24), and then the fitness function will be estimated. Here, the fitness function uses the cost-revenue function in Equation (14) to estimate its fitness degree by Equation (25). The classical greedy algorithm [48] is used to select the proper solution. Second, the probability P_{p_IABC} is calculated by (26) and the corresponding scout can be selected properly. Third, the solution v_{ij} of the onlooker from the solutions x_{ij} selected depending on P_{p_IABC} will also be computed by (24); and the greedy algorithm will be used again to select the proper solution. Fourth, the abandoned solution of scout will be determined, and a new randomly solution will be considered for them. Fifth, the best solution will be recorded in this round and the iteration counter will be added by 1.

$$v_{ij} = x_{ij} + \text{rand}(-1, 1) (x_{ij} - x_{kj}) \quad (24)$$

$$f_{p_IABC} = \begin{cases} \frac{1}{1 + T1_{p_IABC}} & T1_{p_IABC} \geq 0 \\ \frac{1}{1 + |T1_{p_IABC}|} & \text{else} \end{cases} \quad (25)$$

$$P_{p_IABC} = \frac{f_{p_IABC}}{\sum_{p_IABC=1}^{NP} f_{p_IABC}} \quad (26)$$

where $i = 1, 2, \dots, NP$; $j = 1, 2, \dots, D$, and $k = 1, 2, \dots, NP$; k and j are the randomly chosen indexes, and $k \neq i$; f_{p_IABC} is the fitness function of solution which is proportional to the nectar amount; $T1_{p_IABC}$ is the cost-revenue function of the p_IABC^{th} iteration.

- (c) The iteration computation will be terminated if the iteration counter reach its upper limitation.

The traditional ABC algorithm may have a shallow search depth, a low evolution efficiency of excellent individual, and a high abandon probability of good nectar source. To conquer these drawbacks to some extent, a balanced searching strategy is proposed. Equations (27)–(29) present its computational method. Clearly, during the early iteration computations, $\delta(p_IABC) > \varepsilon(p_IABC)$, this algorithm will have a good global searching ability in that stage; and with the implementation of iteration, the global optimal solution of current population $x_{best,j}$ will avoid the local minimum solution, fasten convergence speed, and keep algorithm to hold the global searching ability to some extent. In that stage, the convergence speed still can high.

$$x_{ij} = x_{ij} + rand(-1, 1) \times (x_{best,j} - x_{ij}) \times \varepsilon(t) + rand(-1, 1) \times (x_{kj} - x_{ij}) \times \delta(t) \quad (27)$$

$$\varepsilon(p_IABC) = \log_2 \left(1 + \frac{p_IABC}{p_IABC_{\max}} \right) \quad (28)$$

$$\delta(p_IABC) = 1 - \varepsilon(p_IABC) \quad (29)$$

where $x_{best,j}$ is the j^{th} dimension component of global optimal solution of current population; $\varepsilon(p_IABC)$ and $\delta(p_IABC)$ are the balanced searching factors, p_IABC is the current iteration number, p_IABC_{\max} is the maximum iteration number.

4. Results and Discussions

A series of test and evaluation experiments are performed to assess the validity and effectiveness of proposed models and methods. All the simulation programs are written by Python (Pycharm2020) in our PC (4.0 GB RAM, 1.70 GHz Intel (R) Core(TM) i3-4005U CPU). To evaluate the effectiveness of proposed system and method, first, an assessment experiment of AGA is made; second, an evaluation experiment of IABC is performed; third, the experiment of multi-UAV optimal mission assignment and path planning for disaster rescue is implemented; finally, some discussions, extended experiments, and applications are illustrated.

4.1. The Evaluation Experiment of AGA

A mission assignment comparison between the GA and our AGA was made. The task assignment for the sole UAV was used for evaluation. Only the air-line distance between mission points was considered for simulation. The all-permutation of mission point was employed as the chromosome coding method. Both an 8 and an 18 mission points tests were considered in the evaluation experiments. The initial population size was 60, the maximum crossover probability was 0.8, the maximum mutation probability was 0.01; and the maximum iteration numbers were 300, 400, and 500. The coordinates of mission point are presented in Table 4. Table 5 shows the comparison results of fitness function and processing time of GA and AGA. Regarding GA and AGA, the fitness function means the difference between the cost function and revenue function (see Equation (16)); thus, the

smaller the fitness function is the better the optimal computation effect will be. From Table 5, our AGA can achieve the better computational performance. The processing time of AGA is larger because it uses more resource for the selection, crossover, and mutation operations. A statistical evaluation of GA and AGA was also performed. After implementing the mission assignment experiment for 50 times [49], we investigated the average minimum and mean fitness functions of GA and AGA when the iteration times were 300, 400, and 500, respectively. Figure 8 gives out the results. From Figure 8, our AGA can acquire better performance. Table 6 illustrates the mission assignment results of GA and AGA: when the number of mission points are small, GA and AGA will get the similar assignment result; while the results will have remarkable differences when the amount of mission point is large.

Table 4. Coordinates of mission point in the AGA evaluation experiment.

Test Experiment 1			
Number of Mission Point	Coordinate of Mission Point	Number of Mission Point	Coordinate of Mission Point
1	(50, 70)	5	(75, 75)
2	(20, 48)	6	(90, 30)
3	(30, 65)	7	(26, 30)
4	(60, 80)	8	(80, 40)
Test Experiment 2			
Number of Mission Point	Coordinate of Mission Point	Number of Mission Point	Coordinate of Mission Point
1	(50, 70)	10	(105, 60)
2	(20, 48)	11	(98, 49)
3	(30, 65)	12	(93, 87)
4	(60, 80)	13	(47, 12)
5	(75, 75)	14	(84, 17)
6	(90, 30)	15	(39, 75)
7	(26, 30)	16	(98, 74)
8	(80, 40)	17	(75, 24)
9	(60, 20)	18	(39, 8)

Table 5. Population evaluation indices comparisons of GA and AGA.

		Fitness Function Value			
		Best Value	Worst Value	Standard Deviation Value	Mean Value
Test experiment 1	GA	203.5649	322.9047	33.6182	261.5839
	AGA	200.8118	286.4434	30.7327	225.2601
Test experiment 2	GA	506.3372	744.7273	56.8380	623.5432
	AGA	369.5323	493.2025	30.5143	429.6063
		Processing Time (s)			
		Best Value	Worst Value	Standard Deviation Value	Mean Value
Test experiment 1	GA	1.61	2.16	0.11	1.75
	AGA	1.92	2.75	0.24	2.49
Test experiment 2	GA	2.1	3.1	0.26	2.59
	AGA	3.36	4.44	0.16	3.86

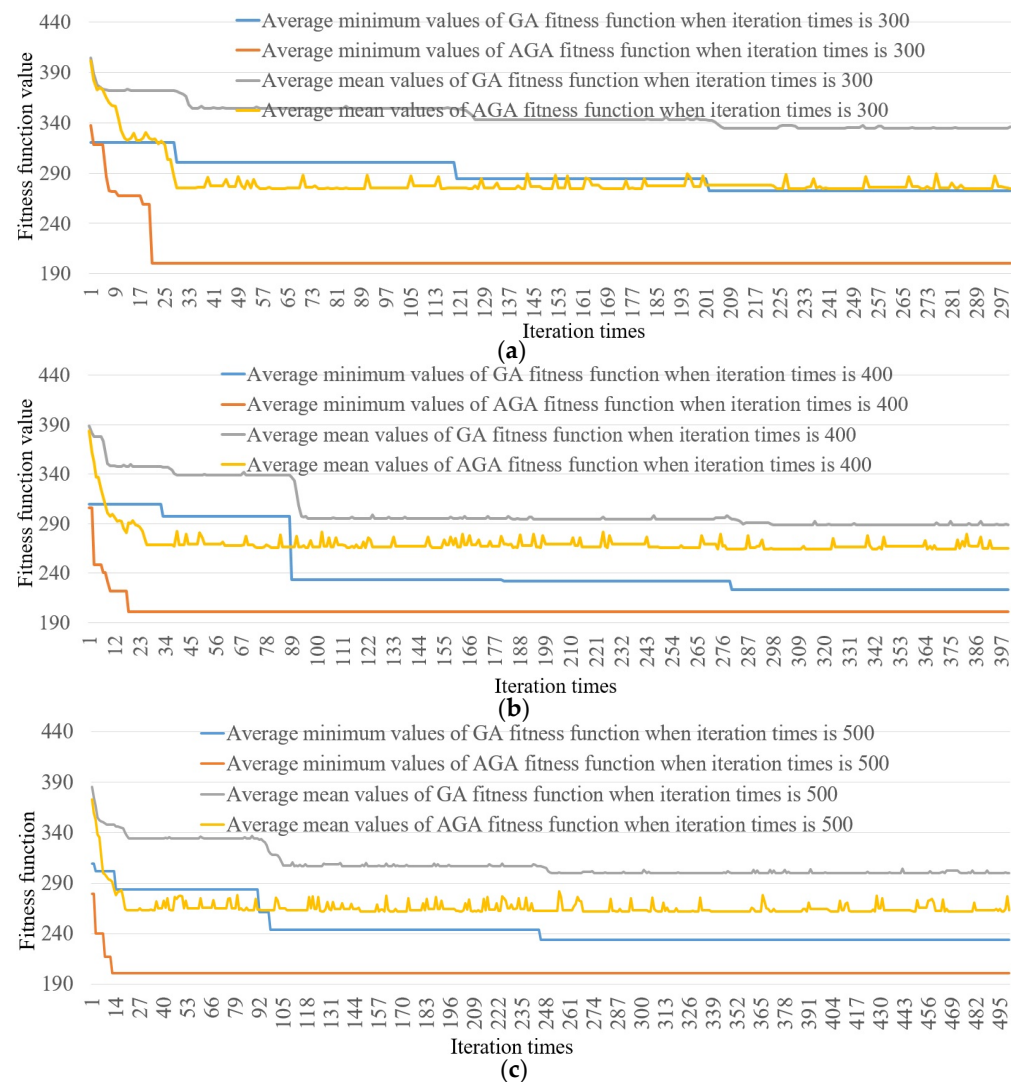


Figure 8. Average minimum and mean fitness function values of GA and AGA when the iteration times are 300, 400, and 500. (a) Statistical evaluation results of fitness function when the iteration times is 300. (b) Statistical evaluation results of fitness function when the iteration times is 400. (c) Statistical evaluation results of fitness function when the iteration times is 500.

Table 6. Evaluation results of GA and AGA using different experiments and iteration times.

		Result of Optimal Mission Point Schedule		
		Iteration Times = 300	Iteration Times = 400	Iteration Times = 500
Test experiment 1	GA	2, 3, 4, 5, 1, 7, 6, 8	2, 7, 3, 1, 5, 4, 8, 6	7, 3, 2, 1, 4, 5, 8, 6
	AGA	7, 2, 3, 1, 4, 5, 8, 6	7, 2, 3, 1, 4, 5, 8, 6	7, 2, 3, 1, 4, 5, 8, 6
Test experiment 2		13, 8, 6, 4, 5, 11, 10, 12,	14, 9, 13, 2, 1, 11, 10, 16,	7, 2, 14, 6, 10, 11, 8, 17,
	GA	16, 17, 9, 2, 1, 15, 3, 18,	17, 18, 7, 15, 3, 4, 5, 12,	9, 13, 18, 16, 12, 15, 1, 3,
		7, 14	8, 6	4, 5
		2, 1, 12, 16, 10, 11, 17,	13, 18, 7, 2, 3, 15, 1, 9,	3, 15, 1, 17, 9, 2, 7, 18,
	AGA	14, 6, 8, 5, 4, 15, 3, 7, 18,	14, 17, 4, 5, 12, 16, 8, 6,	13, 14, 6, 8, 11, 5, 4, 12,
		13, 9	11, 10	16, 10

4.2. The Evaluation Experiment of IABC

An optimal path planning comparison experiment between ABC and IABC was investigated. In this experiment, only the cost function was used to build the fitness function (see (14)). Table 7 presents the parameter settings of threat sources. The initial parameters of ABC and IABC were: the population size was 100; the data dimension was 15;

the coordinates of start and end points were (0, 85) and (120, 30). To assess the performance of ABC and IABC, the optimal fitness function, path length, and processing time were considered. Table 8 presents the corresponding results. Regarding ABC and IABC, the larger the fitness function is the better the algorithm performance will be. Because the IABC employs a balanced searching strategy which adds more amounts of computation, the processing speed of proposed IABC is slow. However, there is no processing time requirement in our application currently, thus the corresponding result is acceptable. Finally, from Table 8, our method can get better fitness function and use less path length, as a result we think its performance is better than the traditional method.

Table 7. Parameters setting methods of threat sources.

Num	Center Coordinate, Radius, Rain State ^a , and Wind Degree of Severe Weather Threat Source	Center Coordinate, ($\mu 1_{i,j,p,1}$, $\sigma 1^2_{i,j,p,1}$), ($\mu 2_{i,j,p,2}$, $\sigma 2^2_{i,j,p,2}$), $w_{j,p,1}$, and $w_{j,p,2}$ of Transmission Tower Threat Source	Center Coordinate, Minimum Height, Maximum Height, and Radius of Upland Threat Source
1	(31, 21), 10, 0, 4	(13, 63), (1, 5), (1, 9), 0.5, 0.5	(38, 48), 150, 300, 13
2	(67, 32), 15, 1, 2	(60, 75), (2, 6), (2, 10), 0.5, 0.5	(88, 77), 150, 300, 10
3	(75, 97), 8, 0, 3	(20, 83), (3, 7), (3, 11), 0.5, 0.5	(70, 60), 150, 300, 6
4	(39, 90), 9, 0, 3	(92, 57), (4, 8), (4, 12), 0.5, 0.5	(101, 25), 150, 300, 14

^a The rain state is: if there is a rain the value will be 1; otherwise the value should be 0.

Table 8. Evaluation results of ABC and IABC using different indices and iteration times.

Iteration Times	Method	Optimal Fitness Function	Path Length	Processing Time
300	ABC	0.8957	172.5320	3.58
	IABC	0.8984	167.8581	5.76
Iteration Times	Method	Optimal Fitness Function	Path Length	Processing Time
400	ABC	0.8980	168.1855	4.51
	IABC	0.8987	167.7283	7.42
Iteration Times	Method	Optimal Fitness Function	Path Length	Processing Time
500	ABC	0.8975	167.4791	5.54
	IABC	0.8987	167.4733	9.03

The simulation results of fitness function, path length, and processing time using different iteration times are illustrated in Table 9. The best, worst, mean, and standard deviation values of fitness function, path length, and processing time of different populations are presented. From Table 9, our IABC can get the larger fitness function, shorter flight path length, while longer processing time. Since the processing time is acceptable (i.e., not important) for our application, our IABC is better than ABC in Table 9. Figures 9–11 present the visualization examples of optimal path planning and the statistical results of fitness function using different iteration times. The total experiment times of ABC and IABC were 30. The best fitness function values of populations in each simulation were used to compute the statistical data in Figures 9–11. From Figures 9–11, the IABC can get smoother flight path and its fitness function indices are larger than those of ABC most of time; therefore, we think our IABC has better performance instead of ABC.

Table 9. Performance evaluation results of ABC and IABC using different iteration times.

Fitness Function/The Iteration Times Is 300				
	Best Value	Worst Value	Standard Deviation Value	Mean Value
ABC	0.8985	0.8943	1.3×10^{-3}	0.8972
IACB	0.8986	0.8967	4.6143×10^{-4}	0.8981
Path Length/The Iteration Times Is 300				
	Best Value	Worst Value	Standard Deviation Value	Mean Value
ABC	167.2298	172.5320	1.3489	168.6910
IACB	164.8105	168.5795	0.97294	167.6903
Processing Time (s)/The Iteration Times Is 300				
	Best Value	Worst Value	Standard Deviation Value	Mean Value
ABC	3.56	4.27	0.1541	3.95
IACB	5.70	6.36	0.1322	6.02
Fitness Function/The Iteration Times Is 400				
	Best Value	Worst Value	Standard Deviation Value	Mean Value
ABC	0.8987	0.8964	5.3594×10^{-4}	0.8982
IACB	0.8988	0.8981	1.7287×10^{-4}	0.8986
Path Length/The Iteration Times is 400				
	Best Value	Worst Value	Standard Deviation Value	Mean Value
ABC	166.6625	169.4589	0.6558	168.2398
IACB	166.5989	168.4041	0.4691	167.8869
Processing Time (s)/The Iteration Times Is 400				
	Best Value	Worst Value	Standard Deviation Value	Mean Value
ABC	5.23	4.53	0.1462	4.70
IACB	7.86	7.55	0.0778	7.68
Fitness Function/The Iteration Times Is 500				
	Best Value	Worst Value	Standard Deviation Value	Mean Value
ABC	0.8987	0.8975	2.8031×10^{-4}	0.8985
IACB	0.8988	0.8982	1.3235×10^{-4}	0.8987
Path Length/The Iteration Times is 500				
	Best Value	Worst Value	Standard Deviation Value	Mean Value
ABC	167.4791	169.0534	0.3398	168.4406
IACB	167.3409	168.5107	0.2934	168.2355
Processing Time (s)/The Iteration Times Is 500				
	Best Value	Worst Value	Standard Deviation Value	Mean Value
ABC	5.29	6.09	0.2080	5.60
IACB	8.83	10.13	0.3193	9.41

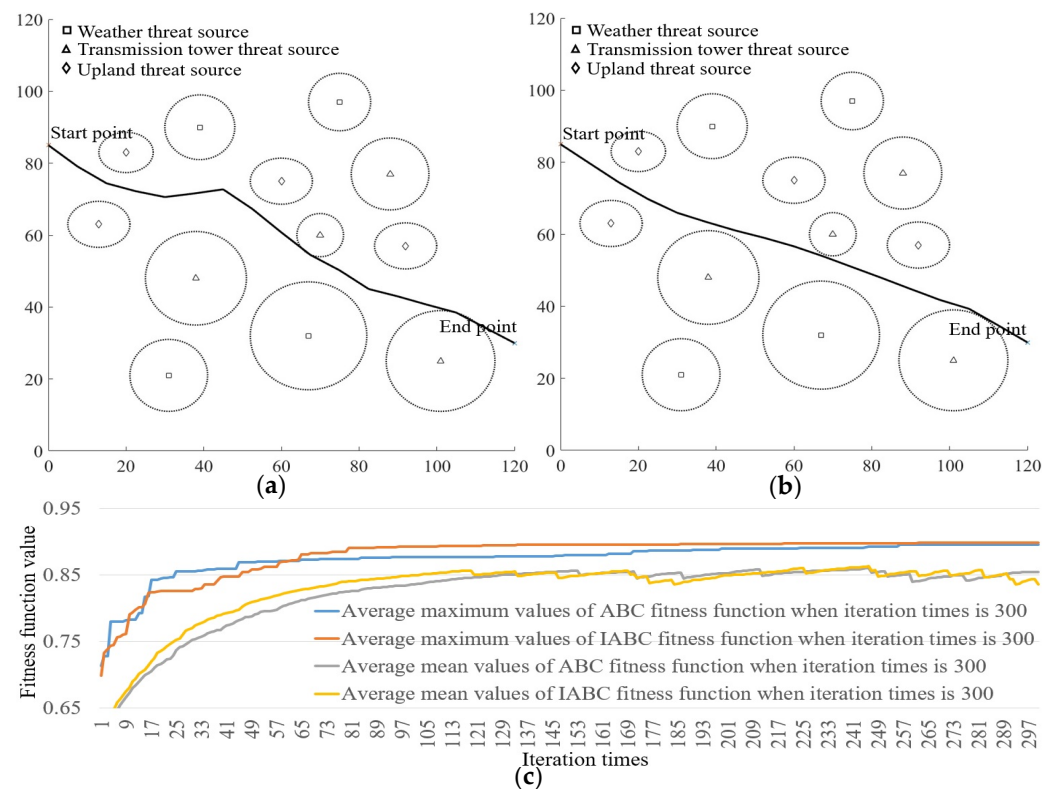


Figure 9. Examples of path planning and statistical results of fitness function using 300 iterations. (a,b) Path planning examples of ABC and IABC when iteration times is 300. (c) Statistical results of fitness function of ABC and IABC when iteration times is 300.

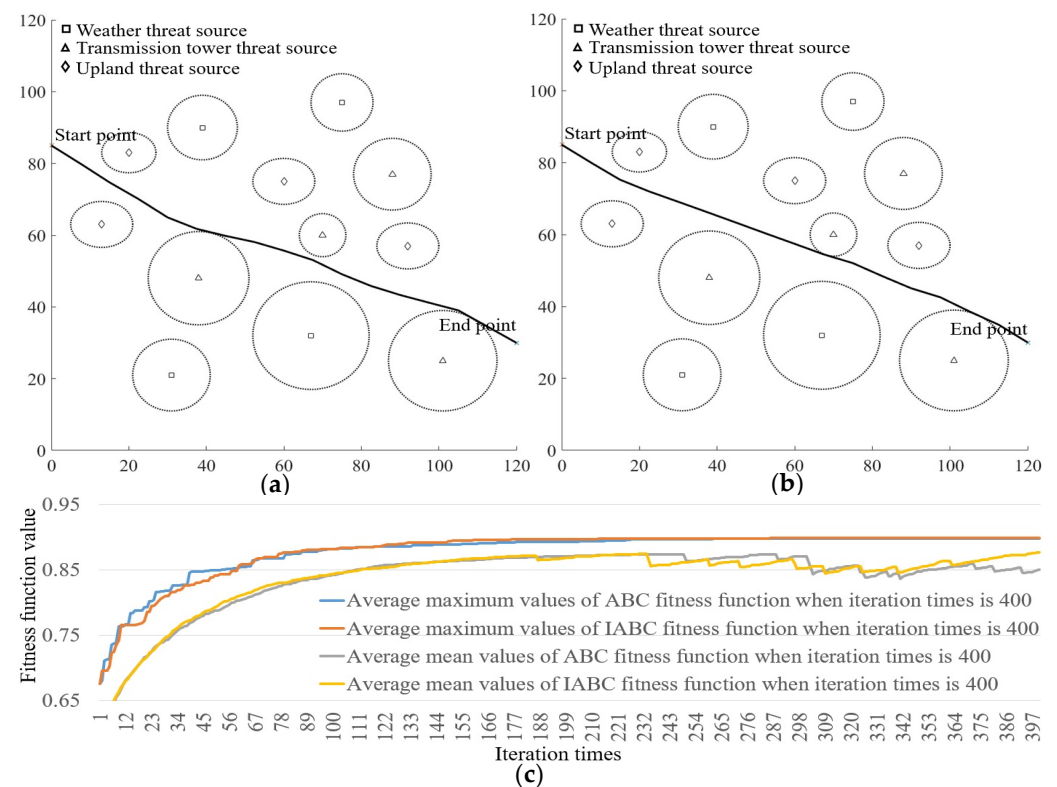


Figure 10. Examples of path planning and statistical results of fitness function using 400 iterations. (a,b) Path planning examples of ABC and IABC when iteration times is 400. (c) Statistical results of fitness function of ABC and IABC when iteration times is 400.

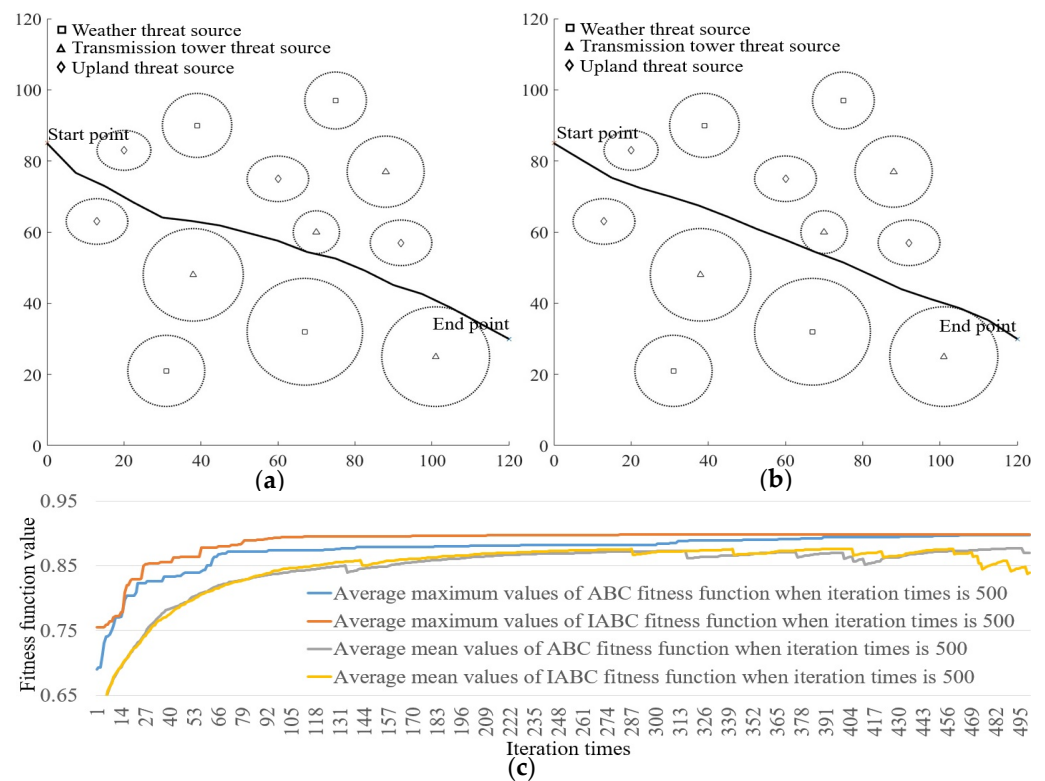


Figure 11. Examples of path planning and statistical results of fitness function using 500 iterations. (a,b) Path planning examples of ABC and IABC when iteration times is 500. (c) Statistical results of fitness function of ABC and IABC when iteration times is 500.

4.3. The Evaluation Experiment of Disaster Rescue Simulation

An evaluation experiment of disaster rescue was performed. The AHP was used to estimate the weights of cost-revenue function in Equations (11) and (12). In this experiment, Tables 10–13 give out the judgmental matrixes of AHP criteria hierarchy of mission point, the judgmental matrixes of UAV performance alternative hierarchy of mission point, the judgmental matrixes of threat source alternative hierarchy of mission point, and the final importance weights of mission point. Tables 14–17 present the corresponding judgmental matrixes and final importance weights of recovery point. Regarding the data in Tables 10–12 and Tables 14–16, the judgmental matrixes come from the advice of disaster rescue experts. From Tables 13 and 17, the weather threat source is the most important factor; while the flight distance is the least important factor for mission points and the oil consumption factor is the least important factor for recovery point. Since the recovery point will always be selected in the site which does not have too many threat sources, this result is reasonable for our application.

Table 10. Judgmental matrixes of AHP criteria hierarchy of mission point.

	Threat Source	UAV Performance
Threat source	1	7
UAV performance	1/7	1

Table 11. Judgmental matrixes of UAV performance alternative hierarchy of mission point.

	Oil Consumption (δ_{MP}^O)	Flight Distance (δ_{MP}^D)
Oil consumption (δ_{MP}^O)	1	9
Flight distance (δ_{MP}^D)	1/9	1

Table 12. Judgmental matrixes of threat source alternative hierarchy of mission point.

	Weather (δ_{MP}^{WR})	Transmission Tower (δ_{MP}^{TT})	Upland (δ_{MP}^{UT})
Weather (δ_{MP}^{WR})	1	9	9
Transmission tower (δ_{MP}^{TT})	1/9	1	1
Upland (δ_{MP}^{UT})	1/9	1	1

Table 13. Final estimated importance weights of AHP of mission point.

Name	δ_{MP}^D	δ_{MP}^O	δ_{MP}^{WR}	δ_{MP}^{TT}	δ_{MP}^{UT}
Value	0.0125	0.1125	0.7159	0.0795	0.0795

Table 14. Judgmental matrixes of AHP criteria hierarchy of recovery point.

	Threat Source	UAV Performance
Threat source	1	3
UAV performance	1/3	1

Table 15. Judgmental matrixes of UAV performance alternative hierarchy of recovery point.

	Oil Consumption (δ_{RP}^O)	Flight Distance (δ_{RP}^D)
Oil consumption (δ_{RP}^O)	1	6
Flight distance (δ_{RP}^D)	1/6	1

Table 16. Judgmental matrixes of threat source alternative hierarchy of recovery point.

	Weather (δ_{RP}^{WR})	Transmission Tower (δ_{RP}^{TT})	Upland (δ_{RP}^{UT})
Weather (δ_{RP}^{WR})	1	8	8
Transmission tower (δ_{RP}^{TT})	1/8	1	2
Upland (δ_{RP}^{UT})	1/8	1/2	1

Table 17. Final estimated importance weights of AHP of recovery point.

Name	δ_{RP}^D	δ_{RP}^O	δ_{RP}^{WR}	δ_{RP}^{TT}	δ_{RP}^{UT}
Value	0.2143	0.0357	0.5968	0.094	0.0592

An integrated evaluation of mission assignment and path planning was performed, the initial experiment parameters were: the amounts of drug delivery, image collection, and communication relay UAVs were 15, 3; and 2; the UAVs were classified into two groups; the coordinates of start point of UAV groups were (0, 50) and (0, 52); the coordinate of recovery point was (120, 50); $\alpha = 0.5$, $\beta = 0.1$ and $\gamma = 0.1$; $R(k) = \{1.0, 1.3, 1.2, 1.5, 1.4, 1.2\}$. Other parameters of threat sources, GA, AGA, ABC, and IABC were the same to the parameters in Sections 4.2 and 4.3. The mission point coordinates are shown in Table 18. Table 19 shows the results. In Table 19, methods of GA+ABC, GA+IABC, AGA+ABC, and AGA+IABC are investigated; the results of group assignment, mission assignment, total revenue (see (13)), total cost (see (10)), processing time, and path length are simulated. From Table 19, the AGA+IABC can get the best performance except for the processing time. Figure 12 shows our visualization results. Table 20 illustrates the statistical results of average revenue, average cost, average processing time, and average path length. From Table 20, our AGA+IABC can get the best revenue, the least cost, and the shortest path length most of time; thus we believe this method to be good enough for our application.

Table 18. Coordinates of mission point in the disaster rescue evaluation experiment.

Number of Mission Point	Coordinate of Mission Point	Number of Mission Point	Coordinate of Mission Point	Number of Mission Point	Coordinate of Mission Point
1	(23, 70)	3	(44, 72)	5	(85, 43)
2	(25, 40)	4	(51, 38)	6	(75, 82)

Table 19. Results of multi-UAV optimal mission assignment and path planning using different optimization methods.

Method Name	Group Assignment Result ^a	Mission Assignment Result ^b	Total Revenue Result	Total Cost Result	Processing Time (s)	Path Length
GA+ABC	Group A: 8, 1, 2 Group B: 7, 2, 0	Group A: 1, 3, 6 Group B: 2, 4, 5	79.5684	0.1453	62.27	340.9001
GA+IABC	Group A: 7, 2, 0 Group B: 8, 1, 2	Group A: 2, 4, 5 Group B: 1, 3, 6	79.4320	0.1633	82.44	334.9619
AGA+ABC	Group A: 7, 2, 0 Group B: 8, 1, 2	Group A: 2, 4, 5 Group B: 1, 3, 6	79.5740	0.1435	92.62	337.5118
AGA+IABC	Group A: 7, 2, 0 Group B: 8, 1, 2	Group A: 2, 4, 5 Group B: 1, 3, 6	79.6475	0.1326	113.68	329.1168

^a The group assignment result means the grouping results of drug delivery, image collection, and communication relay UAVs. ^b The Mission assignment result means the flight orders of mission points.

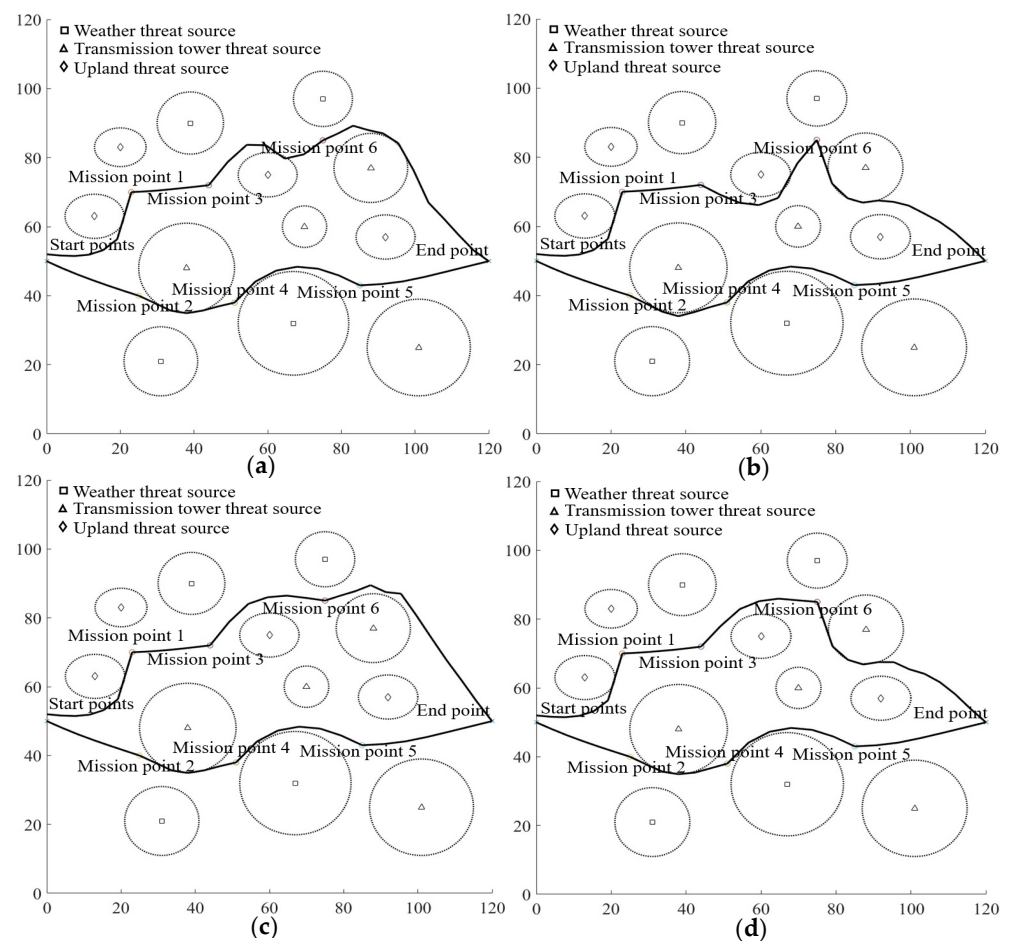
**Figure 12.** Results of multi-UAV optimal mission assignment and path planning using different methods. (a) Visualization results of GA+ABC. (b) Visualization results of GA+IABC. (c) Visualization results of AGA+ABC. (d) Visualization results of AGA+IABC.

Table 20. Statistical results of average revenue, average cost, average processing time, and average path length using different mission assignment and path planning methods.

Average Revenue Result				
	Best Value	Worst Value	Standard Deviation Value	Mean Value
GA+ABC	79.6017	79.1356	0.1157	79.4761
GA+IABC	79.6265	79.3540	0.0706	79.5123
AGA+ABC	79.5799	77.7220	0.5315	79.3207
AGA+IABC	79.6475	79.4919	0.0363	79.5749
Average Cost Result				
	Best Value	Worst Value	Standard Deviation Value	Mean Value
GA+ABC	0.1418	0.1788	0.0105	0.1534
GA+IABC	0.1350	0.1633	0.0072	0.1461
AGA+ABC	0.1374	0.1985	0.0174	0.1530
AGA+IABC	0.1326	0.1489	0.0039	0.1413
Average Processing Time (s)				
	Best Value	Worst Value	Standard Deviation Value	Mean Value
GA+ABC	61.31	69.34	2.1148	64.52
GA+IABC	79.13	86.84	2.1571	83.54
AGA+ABC	89.92	95.73	1.9324	93.08
AGA+IABC	102.24	114.87	3.4733	108.71
Average Path Length				
	Best Value	Worst Value	Standard Deviation Value	Mean Value
GA+ABC	329.5748	340.9091	3.7418	336.6497
GA+IABC	329.8217	343.4356	3.4055	334.4394
AGA+ABC	331.0667	379.0624	12.5883	339.6279
AGA+IABC	328.6109	337.5947	2.7720	331.9636

4.4. Discussions

With the fast technique advancement, the multi-UAV and multi-UAV mission formation [50] have been widely studied to assist the disaster rescue of villages which locate far away from the big city. Currently, the familiar hypothetical rescue task always happens in the southwest China because the earthquake belt crosses this area. The terrain in southwest China always has the basin or karst landform [51] (see Figure 3b), the weather there is rainy and windy most of the year. Thus, it is necessary to make a careful design of task assignment of medical rescue before the serious earthquake damage happens. Comparing with a single UAV, the multiple UAVs can take larger amount of rescue resources, accomplish more rescue functions, and behave better flight stability. Thus, how to assign the proper UAVs for different rescue points and how to plan their flight paths should be studied before the implementation of rescue. To conquer these problems to some extent, an intelligent algorithm is developed in this study which considers the flight factor, the UAV function factor, the threat source factor, and the UAV recovery factor, etc. This research work can be used for the decision support of disaster medical rescue.

Three types of threat source models were considered in this study, i.e., the weather threat source, transmission tower threat source, and upland threat source. The modeling of weather phenomenon really is a complex task because too many factors will affect the local weather, such as the wind, temperature, humidity, sun light, and even the local terrain. In this study, a simplified weather threat source was proposed for a fast computation purpose; only the factors of wind and rain were considered. The influence scope of bad weather was abstracted by a circle around the weather station. In future, the atmosphere temperature model [52] can be researched for our application. The electromagnetic disturbance cannot be omitted for any UAV applications. The manmade disturbance source, i.e., the transmission tower, was modeled in this study. In fact, the power line itself and the nature disturbance

sources (such as the thunder, ground radiation, etc.) can also be studied in future. A simplified upland model was used in our model. The distance from the ground was considered to assess the degree of threat source intensity. Clearly, the 3D terrain model can be used to replace that circular cone in our next research step.

A kind of revenue-cost function was designed to guide the optimal computation of mission assignment and path planning. Both the revenue and cost in the mission point and recovery point were considered. The revenue function reflects the rescue value of typical mission point (i.e., the village); the larger the revenue function value is the better the optimal computation will be. The cost function indicates the risk, material cost, and mission complexity during the disaster rescue; the smaller the cost function value is the better the model computation effect will be. The function assignment of UAVs is controlled by the parameters in the revenue and cost functions. In this study, the flight distance, oil consumption, UAV function descriptions, threat source factors, and mission point revenue participated the construction of revenue-cost function. To improve the modeling objectivity, the AHP model was used to estimate the weights of revenue-cost function. The opinions of disaster rescue experts were used to build the AHP model. The meeting discussion can be considered for expert opinion collection. Clearly, more factors can be considered in the design of revenue-cost function in future, such as the minimum turning radius of UAV, precision of satellite navigation, and other threat source factors, etc.

Both an AGA and an IABC [53] were developed for mission assignment and path planning in the disaster rescue task. Regarding the mission assignment, the GA-based method [54,55] has been proofed to be the best scheduling method in our former research; thus it is not necessary to consider other techniques for solving this task. Differently, as for the path planning problem, many other optimization methods can be considered, such as the particle swarm optimization (PSO) [56] method, artificial potential field algorithm (APFA) [57], or bat algorithm [58], etc. After a series of tests, it can be found the performance of bat algorithm cannot fulfill our application requirement; thus, only the PSO and APFA were evaluated. Figure 13 presents the visualization results of multi-UAV optimal mission assignment and path planning using GA, AGA, PSO, and APFA. From Figure 13, the PSO-based method can get a smoother flight path. Table 21 gives out the statistical evaluation result of average revenue, average cost, average processing time, and average path length using GA, AGA, PSO, and APFA. The simulation times was 40. From Table 21, similar to the results in Table 20, the methods of AGA+PSO and AGA+APFA can get better performances than the methods of GA+PSO and GA+APFA, respectively. These results can illustrate the effectiveness of proposed AGA to some extent.

A series of evaluation experiments were performed to assess the effect of proposed computational method in this study. Many evaluation indices, such as the statistical value of fitness function, iteration times, or program processing time, were used. For example, regarding the IABC algorithm, it needs more computational resource for the computation of balanced searching strategy (see Equations (27)–(29)) than the ABC method; however its convergence speed is faster than ABC. The experiment results showed if we investigated the algorithm performance of 1000 iterations, the convergence times (i.e., the value of fitness function would not be changed) of ABC and IABC were 440 and 316, respectively; and the processing time of ABC and IABC were 12.1826 s and 15.0539 s; thus, the average convergence time of ABC and IABC were 5.3603 s and 4.757 s, respectively. As for the iteration times in the GA and AGA evaluation experiments, the larger the iteration times is the smaller the fitness function will be (see Figure 8). When it comes to the iteration times of ABC and IABC, the path length will decrease firstly and then increase slightly with the rise of iteration times; and the fitness function will increase, the processing time will rise distinctly. Clearly, all these results can illustrate the good performance of our proposed methods.

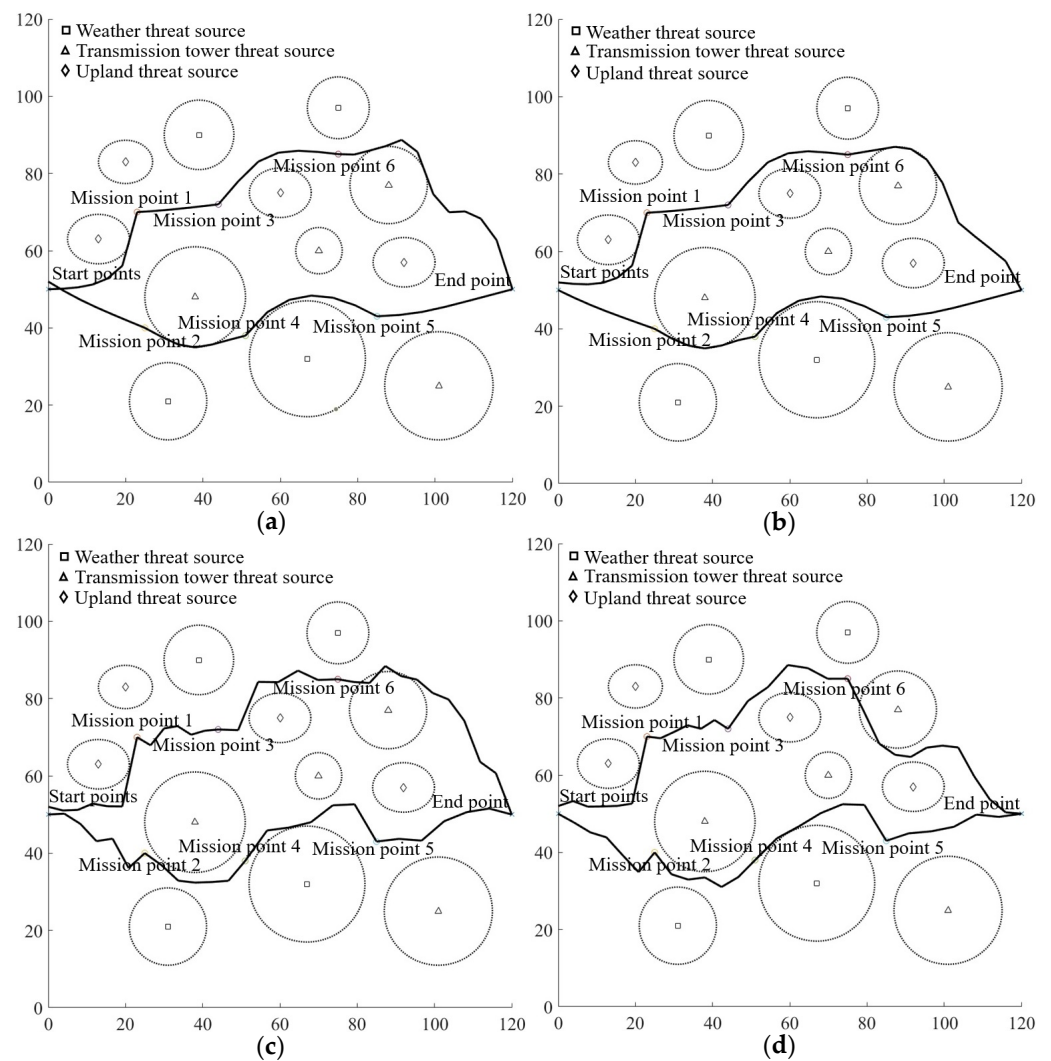
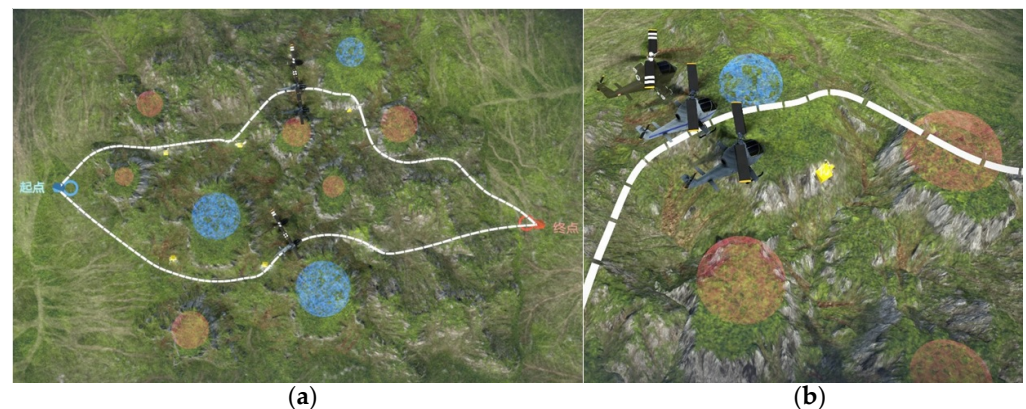


Figure 13. Visualization results of multi-UAV optimal mission assignment and path planning using GA, AGA, PSO, and APFA. (a) Visualization results of GA+PSO. (b) Visualization results of AGA+PSO. (c) Visualization results of GA+APFA. (d) Visualization results of GA+APFA.

The proposed algorithm can be used for practical application. An optimal computation module together with a visualization simulation software [59] were developed for the disaster rescue task in our application. Currently, both the fixed wing UAV and the multi-rotor unmanned helicopter can be used for this application. In our software, the 3D terrain came from the satellite remote sensing data. Figure 14 presents the corresponding visualization results. In Figure 14, the color 3D terrain is illustrated; the optimal paths are presented by the white dash lines; the threat sources are marked by the hemispheres with blue or red color; and multiple helicopters are also displayed in that scene. In Figure 14, the UAVs are classified into two groups. Regarding this software, because the optimal computation will cost too much time, as a result the optimal mission assignment and path planning will be computed firstly, and then the corresponding results will be displayed by the 3D visualization program. Another issue in this study is: the height information of UAV is not considered in our model; this designing comes from the fact that the UAV uses the altimeter to control its flight height from the ground; and in many cases its flight height can be a fixed value.

Table 21. Statistical evaluation results of average revenue, average cost, average processing time, and average path length using GA, AGA, PSO, and APFA.

Average Revenue Result				
	Best Value	Worst Value	Standard Deviation Value	Mean Value
GA+PSO	79.5746	77.4224	0.7295	79.0008
AGA+PSO	79.5918	78.0337	0.3909	79.3464
GA+APFA	79.4929	77.5304	0.5118	79.0061
AGA+APFA	79.5426	78.9268	0.1757	79.3605
Average Cost Result				
	Best Value	Worst Value	Standard Deviation Value	Mean Value
GA+PSO	0.1444	0.2815	0.0317	0.1615
AGA+PSO	0.1411	0.1919	0.0170	0.1533
GA+APFA	0.1445	0.1847	0.0116	0.1601
AGA+APFA	0.1419	0.1721	0.0083	0.1508
Average Processing Time (s)				
	Best Value	Worst Value	Standard Deviation Value	Mean Value
GA+PSO	112.47	120.24	115.82	2.8234
AGA+PSO	178.92	188.56	185.02	1.8648
GA+APFA	1694.52	1798.42	30.5664	1740.98
AGA+APFA	1802.07	1892.88	25.0210	1855.64
Average Path Length				
	Best Value	Worst Value	Standard deviation Value	Mean Value
GA+PSO	329.8403	397.2150	19.3590	352.9970
AGA+PSO	330.4529	344.4585	14.9107	350.3686
GA+APFA	364.3596	432.0467	16.3501	379.0128
AGA+APFA	358.4359	379.2276	6.5640	367.8603

**Figure 14.** Visualization simulation examples of proposed method. (a) Global field view of simulation result. (b) Local field view of simulation result.

The proposed algorithm has at least three advantages. First, our model considers the practical engineering application of disaster rescue carefully. As we have stated above, this method is designed for the medical rescue in southwest China. The typical terrain, weather condition, and artificial facility [60] are all considered when constructing the corresponding target functions. The typical multiple UAVs for the medical disaster rescue are also designed. The function characters of multi-UAV are also proposed for the optimal computation. Second, its computational precision is comparable high. Comparing with other application, an integrated evaluation of mission assignment and path planning is performed. This processing method can refine our computational result. Third, the model

extensibility is good. Clearly, any other optimal methods can be used easily in our computational framework; this system and method can be popularized for any applications outside China only with limited model adjustments. Our algorithm also has some shortcomings. For example, the models of threat sources can be improved and the human-computer interactivity of this system is limited. In future more intelligent techniques can be used in our model.

5. Conclusions

In this study, a multi-UAV mission assignment and path planning method is proposed for the disaster medical rescue. The multiple UAVs include the drug delivery UAV, image collection UAV, and communication relay UAV. Three kinds of threat source models are considered: the severe weather, transmission tower, and upland. When building the cost-revenue function of optimization model, the flight distance, oil consumption, UAV function, and threat sources are utilized. The AHP model is utilized to estimate the weights in this model. Both the cost-revenue functions for the mission point and recovery point are designed. An AGA is designed to solve the optimal mission assignment for mission points; a fitness function which considers the current and maximum iteration numbers are employed to improve the algorithm convergence performance. An IABC method is considered to solve the optimal path planning between the neighboring mission points; a balanced searching strategy is developed to improve the algorithm computational effect. Many evaluation results have proofed the effect of proposed model. This research work can be used for decision support of disaster medical rescue in future.

Author Contributions: Conceptualization, H.L., J.G., J.L. (Jiacheng Li), K.D., Z.Z., Z.G., W.L. and J.L. (Jinhui Lan); Data curation, H.L.; Formal analysis, H.L., J.G., J.L. (Jiacheng Li), K.D., Z.Z., Z.G., W.L. and J.L. (Jinhui Lan); Funding acquisition, H.L.; Investigation, H.L., J.G., K.D., Z.Z. and J.L. (Jinhui Lan); Methodology, H.L., J.G., Y.W., J.L. (Jiacheng Li), K.D., Z.Z., Z.G. and W.L.; Project administration, K.D.; Resources, Z.Z.; Software, Y.W. and J.L. (Jiacheng Li); Supervision, H.L.; Validation, H.L., J.G., Y.W., J.L. (Jiacheng Li), Z.G. and J.L. (Jinhui Lan); Visualization, J.G., Y.W., J.L. (Jiacheng Li) and W.L.; Writing—Original draft, H.L.; Writing—Review & Editing, H.L. All authors have read and agreed to the published version of the manuscript.

Funding: This work was supported by the Fund of Science and Technology on Near-Surface Detection Laboratory under Grant TCGZ2019A003, the National Natural Science Foundation of China under Grant 61975011, the Fund of State Key Laboratory of Intense Pulsed Radiation Simulation and Effect under Grant SKLIPR2024, and the Fundamental Research Fund for the China Central Universities of USTB under Grant FRF-BD-19-002A. The authors declare no conflict of interest.

Conflicts of Interest: The authors declare no conflict of interest.

Abbreviations

Here is a list with the main abbreviations used in this article.

ABC	Artificial bee colony
AGA	Adaptive Genetic algorithm
AHP	Analytic hierarchy process
APFA	Artificial potential field algorithm
GA	Genetic algorithm
GMM	Gaussian mixed model
IABC	Improved artificial bee colony
LES	Large Eddy Simulations
PC	Personal computer
PSO	Particle swarm optimization
UAV	Unmanned aerial vehicle
WRF	Weather research and forecasting

Nomenclature

$P_{i,j,p,WR}$	The threat degree of rain and wind of the i^{th} UAV in the j^{th} threat source under the p^{th} iterative computation.
$P_{i,j,p,R}$	The threat degree of rain of the i^{th} UAV in the j^{th} threat source under the p^{th} iterative computation.
$P_{i,j,p,W}$	The threat degree of wind of the i^{th} UAV in the j^{th} threat source under the p^{th} iterative computation.
d_{WR}	The distance between UAV and weather threat source center.
D_{WR}	The radius of weather threat source.
$P_{i,p,WR}$	The integrated weather threat degree of the i^{th} UAV under the p^{th} iterative computation.
M_1	The total amount of weather threat source.
$f_{i,j,p,q}(x, y)$	The probability density function of bi-GMM function of the i^{th} UAV in the j^{th} threat source under the p^{th} iterative computation, q is the number of Gaussian function.
$\mu 1_{i,j,p,q}$	The mean of Gaussian function 1 of the i^{th} UAV in the j^{th} threat source under the p^{th} iterative computation, q is the number of Gaussian function.
$\mu 2_{i,j,p,q}$	The mean of Gaussian function 2 of the i^{th} UAV in the j^{th} threat source under the p^{th} iterative computation, q is the number of Gaussian function.
$\sigma 1_{i,j,p,q}$	The variance of Gaussian function 1 of the i^{th} UAV in the j^{th} threat source under the p^{th} iterative computation, q is the number of Gaussian function.
$\sigma 2_{i,j,p,q}$	The variance of Gaussian function 2 of the i^{th} UAV in the j^{th} threat source under the p^{th} iterative computation, q is the number of Gaussian function.
$\rho_{i,j,p,q}$	The correlation coefficient of bi-GMM of the i^{th} UAV in the j^{th} threat source under the p^{th} iterative computation, q is the number of Gaussian function.
$P_{i,j,p,TT}$	The threat degree of transmission tower of the i^{th} UAV in the j^{th} threat source under the p^{th} iterative computation.
$\omega_{j,p,q}$	The weight of Gaussian function, j is the number of threat source, p is number of iteration times, q is the number of Gaussian function.
$P_{i,p,TT}$	The integrated transmission tower threat degree of the i^{th} UAV in the p^{th} threat source.
M_2	The total number of transmission tower in the investigated area.
$\theta_{i,j,p}$	Please see the definition in Figure 5.
$\frac{A_{i,j,p} O_{i,j,p,m}}{C_{i,j,p} O_{i,j,p,m}}$	Please see the definition in Figure 5.
$\frac{B_{i,j,p} O_{i,j,p,t}}{O_{i,j,p,t} O_{i,j,p,m}}$	Please see the definition in Figure 5.
$\frac{E_{i,j,p} F_{i,j,p}}{G_{i,j,p} H_{i,j,p}}$	Please see the definition in Figure 5.
$\frac{C_{i,j,p} D_{i,j,p}}{C_{i,j,p} D_{i,j,p}}$	Please see the definition in Figure 5.
$P_{i,j,p,UT}$	The threat degree of upland of the i^{th} UAV in the j^{th} threat source under the p^{th} iterative computation.
$P_{i,p,UT}$	The integrated threat degree of upland of the i^{th} UAV under the p^{th} iterative computation.
$C_{i,p,Total}$	The total cost and revenue of the i^{th} UAV in the p^{th} iterative computation.
$C_{i,p,MP}$	The mission point cost function of the i^{th} UAV under the p^{th} iterative computation.
$C_{i,p,RP}$	The recovery point cost function of the i^{th} UAV under the p^{th} iterative computation.
δ_{MP}^D	The weight of distance factor of mission point.
δ_{MP}^O	The weight of oil consumption factor of mission point.
δ_{MP}^{WR}	The weight of weather threat factor of mission point.
δ_{MP}^{TT}	The weight of transmission tower threat factor of mission point.
δ_{MP}^{UT}	The weight of upland threat factor of mission point.
K	The total number of mission point.

δ_{RP}^D	The weight of distance factor of recovery point.
δ_{RP}^O	The weight of oil consumption factor of recovery point.
δ_{RP}^{WR}	The weight of weather threat factor of recovery point.
δ_{RP}^{TT}	The weight of transmission tower threat factor of recovery point.
δ_{RP}^{UT}	The weight of upland threat factor of recovery point.
$P_{i,p,D}(k)$	The distance cost value of mission point k of the i^{th} UAV under the p^{th} iterative computation.
$P_{i,p,O}(k)$	The oil consumption cost value of mission point k of the i^{th} UAV under the p^{th} iterative computation.
$P_{i,p,WR}(k)$	The weather cost value of mission point k of the i^{th} UAV under the p^{th} iterative computation.
$P_{i,p,TT}(k)$	The transmission tower cost value of mission point k of the i^{th} UAV under the p^{th} iterative computation.
$P_{i,p,UT}(k)$	The upland cost value of mission point k of the i^{th} UAV under the p^{th} iterative computation.
$P_{i,p,D}(c)$	The distance cost value of recovery point c of the i^{th} UAV under the p^{th} iterative computation.
$P_{i,p,O}(c)$	The oil consumption cost value of recovery point c of the i^{th} UAV under the p^{th} iterative computation.
$P_{i,p,WR}(c)$	The weather cost value of recovery point c of the i^{th} UAV under the p^{th} iterative computation.
$P_{i,p,TT}(c)$	The transmission tower cost value of recovery point c of the i^{th} UAV under the p^{th} iterative computation.
$P_{i,p,UT}(c)$	The upland cost value of recovery point c of the i^{th} UAV under the p^{th} iterative computation.
r_p	The amount of drug delivery UAV under the p^{th} iterative computation.
s_p	The amount of image collection UAV under the p^{th} iterative computation.
t_p	The amount of communication relay UAV under the p^{th} iterative computation.
α	The rate of successful drug delivery of drug delivery UAV.
β	The improvement probability of drug delivery caused by image collection UAV.
γ	The decreasing probability of threat source caused by communication relay UAV.
$R(k)$	The revenue of the k^{th} mission point.
ω_1	The weight of Gaussian function 1.
ω_2	The weight of Gaussian function 2.
I	The total amount of UAV.
f_{p_AGA}	The fitness function of AGA under the p_AGA^{th} iteration.
$T2_{p_AGA}$	The AGA application of Equation (15).
$P_{p_AGA,S}$	The selection probability of AGA under the p_AGA^{th} iteration.
N_AGA	The maximum population amount of AGA.
$P_{p_AGA,C}$	The cross probability of AGA under the p_AGA^{th} iteration.
a_{p_AGA}	A control parameter of AGA fitness function under the p_AGA^{th} iteration.
b_{p_AGA}	A control parameter of AGA fitness function under the p_AGA^{th} iteration.
c_{p_AGA}	A control parameter of AGA fitness function under the p_AGA^{th} iteration.
d_{p_AGA}	A control parameter of AGA fitness function under the p_AGA^{th} iteration.
P_{p_AGA,C_max}	The maximum of cross probability of AGA under the p_AGA^{th} iteration.
$f_{p_AGA,max}$	The maximum of fitness function of AGA under the p_AGA^{th} iteration.
$f_{p_AGA,mean}$	The mean of fitness function of AGA under the p_AGA^{th} iteration.
$P_{p_AGA,M}$	The mutation probability of AGA under the p_AGA^{th} iteration.
$P_{p_AGA,M,max}$	The maximum of mutation probability of AGA under the p_AGA^{th} iteration.
K_{AGA}	The adjustment parameter of fitness function of AGA.
h_i	The iteration times-related variable of AGA algorithm.
$T2_{p_AGA}^{\max}$	The maximum of cost-revenue function under the p_AGA^{th} iteration.
p_AGA_{\max}	The maximum iteration number of AGA.
x_{ij}	The coordinate of flight path.
x_j^{\min}	The minimum value of x_{ij} .
x_j^{\max}	The maximum value of x_{ij} .

NP	The total amount of bee of ABC algorithm.
D	The parameter dimension of ABC algorithm.
f_{p_IABC}	The fitness function of IABC algorithm.
$T1_{p_IABC}$	The cost-revenue function of IABC algorithm under p_IABC^{th} iteration.
$x_{best,j}$	The j^{th} dimension component of global optimal solution of current population.
$\varepsilon(p_IABC)$	The balanced searching factor 1 of IABC algorithm.
$\delta(p_IABC)$	The balanced searching factor 2 of IABC algorithm.
p_IABC	The current iteration number of IABC algorithm.
p_IABC_{\max}	The maximum iteration number of IABC algorithm.

References

- Liu, H.; Yan, B.; Wang, W.; Li, X.; Guo, Z. Manhole cover detection from natural scene based on imaging environment perception. *KSII Trans. Internet Inf.* **2019**, *13*, 5059–5111.
- Lv, M.; Zheng, J.; Tong, Q.; Chen, J.; Liu, H.; Gao, Y. Modeling and simulation of scheduling medical materials using graph model for complex rescue. *J. Inf. Process. Syst.* **2017**, *13*, 1243–1258.
- Chen, J.; Liu, H.; Zheng, J.; Lv, M.; Yan, B.; Hu, X.; Gao, Y. Damage degree evaluation of earthquake area using UAV aerial image. *Int. J. Aerosp. Eng.* **2016**, *216*, 2052603. [\[CrossRef\]](#)
- Liu, H.; Wang, W.; He, Z.; Tong, Q.; Wang, X.; Yu, W.; Lv, M. The design of air-space integrative calamity information analysis and rescue system. In Proceedings of the IEEE International Conference on Cyber Technology in Automation, Control and Intelligent Systems, Shenyang, China, 8–12 June 2015; pp. 1997–2001.
- Yamazaki, F.; Miyazaki, S.; Liu, W. 3D visualization of landslide affected area due to heavy rainfall in Japan from UAV flights and SfM. In Proceedings of the IEEE International Geoscience and Remote Sensing Symposium, Valencia, Spain, 22–27 July 2018; pp. 5685–5688.
- Fan, Q.; Wang, F.; Shen, X.; Luo, D. Path planning for a reconnaissance UAV uncertain environment. In Proceedings of the IEEE International Conference on Control and Automation, Kathmandu, Nepal, 1–3 June 2016; pp. 248–252.
- Hao, R.; Luo, D.; Duan, H. Multiple UAVs mission assignment based on modified pigeon-inspired optimization algorithm. In Proceedings of the IEEE Chinese Guidance, Navigation and Control Conference, Yantai, China, 8–10 August 2014; pp. 2692–2697.
- He, Z.; Zhao, L. The comparison of four UAV path planning algorithms based on geometry search algorithm. In Proceedings of the International Conference on Intelligent Human-Machine Systems and Cybernetics, Hangzhou, China, 26–27 August 2017; pp. 33–36.
- Cichella, V.; Kaminer, I.; Dobrokhodov, V.; Xargay, E.; Choe, R.; Hovakimyan, N.; Pedro Aguiar, A.; Pascoal, A.M. Cooperative path following of multiple multirotors over time-varying networks. *IEEE Trans. Autom. Sci. Eng.* **2015**, *12*, 945–957. [\[CrossRef\]](#)
- Oh, H.; Turchi, D.; Kim, S.; Tsourdos, A.; Pollini, L.; White, B. Coordinated standoff tracking using path shaping for multiple UAVs. *IEEE Trans. Aerosp. Electron. Syst.* **2014**, *50*, 348–363. [\[CrossRef\]](#)
- Nguyen, H.V.; Rezatofighi, H.; Vo, B.-N.; Ranasinghe, D.C. Online UAV path planning for joint detection and tracking of multiple radio-tagged objects. *IEEE Trans. Signal Process.* **2019**, *67*, 5365–5379. [\[CrossRef\]](#)
- Xia, S.; Zhang, X. Constrained path planning for unmanned aerial vehicle in 3D terrain using modified multi-objective particle swarm optimization. *Actuators* **2021**, *10*, 255. [\[CrossRef\]](#)
- Shahzad, A.; Ur-Rehman, R. An artificial intelligence based novel approach for real-time allocation of armament to hostile targets. In Proceedings of the 10th International Bhurban Conference on Applied Sciences & Technology, Islamabad, Pakistan, 15–19 January 2013; pp. 141–146.
- Huang, T.; Wang, Y.; Cao, X.; Xu, D. Multi-UAV mission planning method. In Proceedings of the 3rd International Conference on Unmanned Systems, Harbin, China, 27–28 November 2020; pp. 325–330.
- Luo, W. An efficient sensor-mission assignment algorithm based on dynamic alliance and quantum genetic algorithm in wireless sensor networks. In Proceedings of the International Conference on Intelligent Computing and Integrated Systems, Guilin, China, 22–24 October 2010; pp. 854–857.
- Fan, H.; Liu, F.; Xia, L. Cluster label aligning algorithm based on programming model. In Proceedings of the 24th Chinese Control and Decision Conference, Taiyuan, China, 23–25 May 2012; pp. 1768–1772.
- Ahner, D.; Parson, C. Weapon tradeoff analysis using dynamic programming for a dynamic weapon target assignment problem within a simulation. In Proceedings of the Winter Simulations Conference, Washington, DC, USA, 8–11 December 2013; pp. 2831–2841.
- Dumka, S.; Maheshwari, S.; Kala, R. Decentralized multi-robot mission planning using evolutionary computation. In Proceedings of the IEEE Congress on Evolutionary Computation, Rio de Janeiro, Brazil, 8–13 July 2018; pp. 1–8.
- Kang, S.; Li, J.; Li, J.; Xiong, J.; Liu, C. Application of the evolutionary algorithms for task allocation in uncertain environments with stochastic tuning. In Proceedings of the International Conference on Artificial Intelligence, Information Processing and Cloud Computing, Hangzhou, China, 26–28 June 2021; pp. 1–7.
- Wang, G.; Li, M.; Deng, Z.; Yang, B.; Yao, W. A new approach to solve the mission assignment problem for cooperative UCAVs using immune particle swarm optimizations. In Proceedings of the 10th World Congress on Intelligent Control and Automation, Beijing, China, 6–8 July 2012; pp. 549–554.

21. Mokrane, A.; Choukchou Braham, A.; Cherki, B. UAV path planning based on dynamic programming algorithm on photogrammetric DEMs. In Proceedings of the International Conference on Electrical Engineering, Istanbul, Turkey, 25–27 September 2020; pp. 1–5.
22. Jing, W.; Feng, D.; Zhang, P.; Zhang, S.; Lin, S.; Tang, B. A multi-objective optimization-based path planning method for parallel parking of autonomous vehicle via nonlinear programming. In Proceedings of the 15th International Conference on Control, Automation, Robotics and Vision, Singapore, 18–21 November 2018; pp. 1665–1670.
23. He, N.; Su, Y.; Guo, J.; Fan, X.; Liu, Z.; Wang, B. Dynamic path planning of mobile robot based on artificial potential field. In Proceedings of the International Conference on Intelligent Computing and Human-Computer Interaction, Sanya, China, 4–6 December 2020; pp. 259–264.
24. Chen, Z.; Xu, B. AGV path planning based on improved artificial potential field method. In Proceedings of the IEEE International Conference on Power Electronics, Computer Applications, Shenyang, China, 22–24 January 2021; pp. 32–37.
25. Guo, Q.; Zhang, Z.; Xu, Y. Path-planning of automated guided vehicle based on improved Dijkstra algorithm. In Proceedings of the 29th Chinese Control and Decision Conference, Chongqing, China, 28–30 May 2017; pp. 7138–7143.
26. Li, X.; Hu, X.; Wang, Z.; Du, Z. Path planning based on combination of improved A-star algorithm and DWA algorithm. In Proceedings of the 2nd International Conference on Artificial Intelligence and Advanced Manufacture, Manchester, UK, 15–17 October 2020; pp. 99–103.
27. Chen, X.; Chen, X.-M. The UAV dynamic path planning algorithm research based on Voronoi diagram. In Proceedings of the 26th Chinese Control and Decision Conference, Changsha, China, 31 May–2 June 2014; pp. 1069–1071.
28. Santiago, R.M.C.; De Ocampo, A.L.; Ubando, A.T.; Bandala, A.A.; Dadios, E.P. Path planning for mobile robots using genetic algorithm and probabilistic roadmap. In Proceedings of the IEEE 9th International Conference on Humanoid, Nanotechnology, Information Technology, Communication and Control, Environment and Management, Manila, Philippines, 1–3 December 2017; pp. 1–5.
29. Liu, Z.; Kong, J. Path planning of parafoil system based on particle swarm optimization. In Proceedings of the International Conference on Computational Intelligence and Natural Computing, Wuhan, China, 6–7 June 2009; pp. 450–453.
30. Tang, J.; Zhao, Y.; Li, F. On the use of ant colony algorithm with weighted penalty strategy to optimize path searching. In Proceedings of the International Conference on Intelligent Computing, Automation and Systems, Chongqing, China, 11–13 December 2020; pp. 309–312.
31. Pierpaoli, P.; Egerstedt, M.; Rahmani, A. Altering UAV flight path by threatening collision. In Proceedings of the Digital Avionics Systems Conference, Prague, Czech Republic, 13–17 September 2015; pp. 1–13.
32. Yaraghi, N.; Tabesh, P.; Guan, P.; Zhuang, J. Comparison of AHP and Monte Carlo AHP under different levels of uncertainty. *IEEE Trans. Eng. Manag.* **2015**, *62*, 122–132. [\[CrossRef\]](#)
33. Xhafa, F.; Herrero, X.; Barolli, A.; Takizawa, M. A struggle genetic algorithm for ground stations scheduling problem. In Proceedings of the International Conference on Intelligent Networking and Collaborative Systems, Bucharest, Romania, 19–21 September 2012; pp. 70–76.
34. Wang, Q.; Liu, G.; Guo, K. Research on path planning of UAV based on improved ABC algorithm. *Mach. Tool Hydraul.* **2017**, *45*, 68–72.
35. Gallaher, D.W.; Campbell, G.G.; Meier, W.N. Anomalous variability in Antarctic sea ice extents during the 1960s with the use of nimbus data. *IEEE J.-STARS* **2014**, *7*, 881–887. [\[CrossRef\]](#)
36. Ziouh, A.; Abbou, A.; Marhraoui, S. Efficiency of ripple correlation control compared to fuzzy logic MPPT algorithm in space climate conditions for Nimbus 2 Satellite. In Proceedings of the International Renewable and Sustainable Energy Conference, Tangier, Morocco, 4–7 December 2017; pp. 1–5.
37. Du, P. Ensemble machine learning-based wind forecasting to combine NWP output with data from weather station. *IEEE Trans. Sustain. Energy* **2019**, *10*, 2133–2141. [\[CrossRef\]](#)
38. Mallick, Z.; Kuhn, T.; Korhonen, H.; Kokkola, H.; Laaksonen, A.; Romakkaniemi, S. Effect aerosol concentration and absorbing aerosol on the radiation fog life cycle. *Atmos. Environ.* **2016**, *133*, 26–33. [\[CrossRef\]](#)
39. Wang, Y.; Wang, H.; Xue, H.; Yang, C.; Yan, T. Research on the electromagnetic environment of 110kV six-circuit transmission line on the same tower. In Proceedings of the IEEE PES Innovative Smart Grid Technologies, Tianjin, China, 21–24 May 2012; pp. 1–5.
40. Zheng, T.; Sun, L.; Lou, T.; Guo, X.; Liu, Q. Determination method of safe flight area for UAV inspection for transmission line based on the electromagnetic field calculation. *ShanDong Electr. Power* **2018**, *45*, 27–30.
41. Xu, N.; Shao, X.; Yang, Z. A novel voice morphing system using Bi-GMM for high quality transformation. In Proceedings of the ACIS International Conference on Software Engineering, Artificial Intelligence, Networking, and Parallel/Distributed Computing, Phuket, Thailand, 6–8 August 2008; pp. 485–489.
42. Hu, Z. Research on Some Key Techniques of UAV Path Planning Based on Intelligent Optimization Algorithm. Ph.D. Thesis, Nanjing University of Aeronautics and Astronautics, Nanjing, China, April 2011.
43. Roberge, V.; Tarbouchi, M.; Labonte, G. Comparison of parallel genetic algorithm and particle swarm optimization for real-time UAV path planning. *IEEE Trans. Ind. Inform.* **2013**, *9*, 132–141. [\[CrossRef\]](#)
44. San, K.T.; Lee, E.Y.; Chang, Y.S. The delivery assignment solution for swarms of UAVs dealing with multi-dimensional chromosome representation of genetic algorithm. In Proceedings of the IEEE Annual Ubiquitous Computing, Electronics & Mobile Communication, New York, NY, USA, 20–22 October 2016; pp. 1–7.

45. Lin, C.-J.; Sie, T.-Y.; Chu, W.-L.; Yau, H.-T.; Ding, C.-H. Tracking control of pneumatic artificial muscle-activated robot arm based on sliding-mode control. *Actuators* **2021**, *10*, 66. [\[CrossRef\]](#)
46. Xiong, X.; Dong, L. A self-adaptive genetic algorithm for labeling line drawings of planar objects. *J. Graph.* **2018**, *39*, 1104–1111.
47. Kubicek, J.; Vilimek, D.; Krestanova, A.; Penhaker, M.; Kotalova, E.; Faure-Brac, B.; Noel, C.; Scurek, R.; Augustynek, M.; Cerny, M.; et al. Prediction model of alcohol intoxication from facial temperature dynamics based on K-means clustering driven by evolutionary computing. *Symmetry* **2019**, *11*, 995. [\[CrossRef\]](#)
48. Trongratsameethong, A.; Mitranont, J.L. Exhaustive greedy algorithm for optimizing intermediate result sizes of join queries. In Proceedings of the IEEE/ACIS International Conference on Computer and Information Science, Shanghai, China, 1–3 June 2009; pp. 463–468.
49. Carrano, E.G.; Wanner, E.F.; Takahashi, R.H.C. A multicriteria statistical based comparison methodology for evaluating evolutionary algorithms. *IEEE Trans. Evol. Comput.* **2011**, *15*, 848–870. [\[CrossRef\]](#)
50. Liu, H.; Wang, W.; Wang, X.; Yu, W.; Lv, M. Multiple rotor UAVs formation flight and its application on level evaluation of earthquake damage. In Proceedings of the International Symposium on Computational Intelligence and Design, Hangzhou, China, 13–14 December 2014; pp. 333–336.
51. Zhou, Q.; Luo, Y.; Zhou, X.; Cai, M.; Zhao, C. Response of vegetation to water balance conditions at different time scales across the karst area of southwestern China—a remote sensing approach. *Sci. Total Environ.* **2018**, *645*, 460–470. [\[CrossRef\]](#)
52. Huang, L.; Peng, H.; Liu, L.; Li, C.; Kang, C.; Xie, S. An empirical atmospheric weighted mean temperature model considering the lapse rate function for China. *Acta Geod. Et Cartogr. Sin.* **2020**, *49*, 432–442.
53. Kubicek, J.; Penhaker, M.; Augustynek, M.; Cerny, M.; Oczka, D. Segmentation of articular cartilage and early osteoarthritis based on the fuzzy soft thresholding approach driven by modified evolutionary ABC optimization and local statistical aggregation. *Symmetry* **2019**, *11*, 861. [\[CrossRef\]](#)
54. Bernal-Romero, D.L.; Montoya, O.D.; Arias-Londono, A. Solution of the optimal reactive power flow problem using a discrete-continuous CBGA implemented in the DigSILENT programming language. *Computers* **2021**, *10*, 151. [\[CrossRef\]](#)
55. Montoya, O.D.; Molina-Cabrera, A.; Grisales-Norena, L.F.; Hincapie, R.A.; Granada, A. Improved genetic algorithm for phase-balancing in three-phase distribution networks: A master-slave optimization approach. *Computation* **2021**, *9*, 67. [\[CrossRef\]](#)
56. Cai, Q.; Long, T.; Wang, Z.; Wen, Y.; Kou, J. Multiple paths planning for UAVs using particle swarm optimization with sequential niche technique. In Proceedings of the Chinese Control and Decision Conference, Yinchuan, China, 28–30 May 2016; pp. 4730–4734.
57. Yao, Q.; Zheng, Z.; Qi, L.; Yuan, H.; Guo, X.; Zhao, M.; Liu, Z.; Yang, T. Path planning method with improved artificial potential field—a reinforcement learning perspective. *IEEE Access* **2020**, *8*, 135513–135523. [\[CrossRef\]](#)
58. Chen, D.-F.; Chiu, S.-P.-C.; Cheng, A.-B.; Ting, J.-C. Electromagnetic actuator system using Witty control system. *Actuators* **2021**, *10*, 65. [\[CrossRef\]](#)
59. Potena, C.; Khanna, R.; Nieto, J.; Siegwart, R.; Nardi, D.; Pretto, A. AgriColMap: Aerial-ground collaborative 3D mapping for precision farming. *IEEE Robot. Autom. Lett.* **2019**, *4*, 1086–1092. [\[CrossRef\]](#)
60. Rezinkina, M.; Rezinkin, O.; Lytvynenko, S.; Tomashevskiy, R. Electromagnetic compatibility at UAVs usage for power transmission lines monitoring. In Proceedings of the IEEE International Conference Actual Problems of Unmanned Aerial Vehicles Developments, Kiev, Ukraine, 22–24 October 2019; pp. 157–160.